

Aggregation-Induced Emission Polymers via Reversible-Deactivation Radical Polymerization

Nicholas Teo¹, Bo Fan¹, Aditya Ardana¹, and San Thang¹

¹Monash University

April 20, 2023

Abstract

Aggregation-Induced Emission (AIE) is a unique phenomenon whereby aggregation of molecules induces fluorescence emission as opposed to the more commonly known Aggregation-Caused Quenching (ACQ). AIE has the potential to be utilized in the large-scale production of AIE-active polymeric materials because of their wide range of practical applications such as stimuli-responsive sensors, biological imaging agents, and drug delivery systems. This is evident from the increasing number of publications over the years since AIE was first discovered. In addition, the ever-growing interest in this field has led many researchers around the world to develop new and creative methods in the design of monomers, initiators and crosslinkers, with the goal of broadening the scope and utility of AIE polymers. One of the most promising approaches to the design and synthesis of AIE polymers is the use of the Reversible-Deactivation Radical Polymerization (RDRP) techniques, which enabled the production of well-controlled AIE materials that are often difficult to achieve by other methods. In this review, a summary of some recent works that utilize RDRP for AIE polymer design and synthesis is presented, including (1) the design of AIE-related monomers, initiators/crosslinkers; the achievements in preparation of AIE polymers using (2) Reversible Addition-Fragmentation Chain Transfer (RAFT) technique; (3) Atom Transfer Radical Polymerization (ATRP) technique; (4) other techniques such as Cu(0)-RDRP technique and Nitroxide-Mediated Polymerization (NMP) technique; (5) the possible applications of these AIE polymers and finally (6) a summary/perspective and the future direction of AIE polymers.

REVIEW

Aggregation-Induced Emission Polymers via Reversible-Deactivation Radical Polymerization

Nicholas Kai Shiang Teo, Bo Fan,* Aditya Ardana, San H. Thang*

School of Chemistry, Monash University, Clayton, VIC 3800, Australia

E-mail: bo.fan@monash.edu, san.thang@monash.edu

Abstract

Aggregation-Induced Emission (AIE) is a unique phenomenon whereby aggregation of molecules induces fluorescence emission as opposed to the more commonly known Aggregation-Caused Quenching (ACQ). AIE has the potential to be utilized in the large-scale production of AIE-active polymeric materials because of their wide range of practical applications such as stimuli-responsive sensors, biological imaging agents, and drug delivery systems. This is evident from the increasing number of publications over the years since AIE was first discovered. In addition, the ever-growing interest in this field has led many researchers around the world to develop new and creative methods in the design of monomers, initiators and crosslinkers, with the goal of broadening the scope and utility of AIE polymers. One of the most promising approaches to the design and synthesis of AIE polymers is the use of the Reversible-Deactivation Radical Polymerization (RDRP) techniques, which enabled the production of well-controlled AIE materials that are often difficult to achieve by

other methods. In this review, a summary of some recent works that utilize RDRP for AIE polymer design and synthesis is presented, including (1) the design of AIE-related monomers, initiators/crosslinkers; the achievements in preparation of AIE polymers using (2) Reversible Addition-Fragmentation Chain Transfer (RAFT) technique; (3) Atom Transfer Radical Polymerization (ATRP) technique; (4) other techniques such as Cu(0)-RDRP technique and Nitroxide-Mediated Polymerization (NMP) technique; (5) the possible applications of these AIE polymers and finally (6) a summary/perspective and the future direction of AIE polymers.

KEYWORDS

Aggregation-induced emission, reversible deactivation radical polymerization, reversible addition-fragmentation chain transfer, atom transfer radical polymerization, nitroxide-mediated polymerization

1. Introduction

1.1 AIE and its incorporation into polymers

Fluorescent molecules have shown their great potential in a diverse range of applications since their first discovery, such as for digital technologies, fluorescence molecular tagging, staining biological cells, and probes for detecting environmental variations.^[1-5] Conventionally, fluorescent molecules emit strongly in the molecular or solution state, but experience appreciable effects of photoluminescence (PL) quenching in the aggregated state, which is a well-known concept discovered and termed by Förster as Aggregation-Caused Quenching (ACQ) in 1954.^[6, 7]

In stark contrast to this phenomenon, in 2001, Tang and co-workers discovered a type of special fluorescent molecule that emits poorly in the molecular or diluted state but emits strongly upon radiative excitation in the aggregated state. They coined this phenomenon as Aggregation-Induced Emission (AIE).^[8-12] At that time, only a peculiar class of silole compounds where a molecule, 1-methyl-1,2,3,4,5-pentaphenylsilole (**Figure 1A**), fluoresces strongly only upon aggregation was discovered.^[8] Subsequently, this new phenomenon attracted a significant amount of research attention, leading to the discovery of a series of new molecules with AIE property in the next few years. Meanwhile, the mechanistic understanding of this new phenomenon also became a hot topic in this field.

The competing effect of ACQ and AIE for any given luminophores depends on multiple factors including (but not limited to) molecular structure and composition, molecular behavior when isolated and when in close proximity to other molecules (i.e. aggregated state). Researchers have attempted to rationalize such observations and among the many proposed explanations, the restriction of intramolecular motion (RIM) theory took the throne.^[13-15] This mechanism comprises two parts: restriction of intramolecular rotation (RIR) (**Figure 1B**) and restriction of intramolecular vibration (RIV) (**Figure 1C**). This theory assumes most molecules that underwent ACQ instead of AIE, possess highly coplanar aromatic rings in them, while AIE molecules adopt a “propeller-shaped” structure where the aromatic rings represent the “rotors”, able to rotate freely in the molecular state and promote energy transfer among molecules, hence generating a new path for non-radiative decay.^[16] In the aggregated form, RIM imposed onto the molecules forces energy dissipation to occur via the radiative pathway instead of the standard mechanical energy dissipation pathway, with fluorescence emission. For example as shown in **Figure 2A**, a classic ACQ luminophore *N,N*-dicyclohexyl-1,7-dibromo-3,4,9,10-perylenetetracarboxylic diimide (DDPD) shows an intense color when dissolved in tetrahydrofuran (THF) solution, but forms insoluble aggregates when water was added due to the solubility (free volume) effect,^[3] thus quenching the PL.^[17] Contrary to this observation, AIE luminogens (AIEgens) reverses the effect of ACQ (**Figure 2B**).^[18] A solution of hexaphenylsilole (HPS) in THF displayed extremely low PL owing to the freely rotatable peripheral rings, but shows an intense color when water was added, by forming insoluble aggregates.

Since its first discovery, AIE molecules were believed to have many new applications that cannot be achieved

by conventional fluorescent molecules. However, AIE molecules alone have only limited applications due to their poor mechanical and film-forming properties. Therefore, the need for incorporating AIE components into polymers is considered necessary in many applications, such as in optoelectronic and biomedical applications where luminescent materials are commonly employed as films and aggregates, with properties vastly different from single isolated molecules.^[19] In addition, these AIE molecules can be used as probes when incorporated into aggregates by monitoring their PL intensities, which is especially useful in the field of material science and engineering, where information on reaction mechanisms and processes are of paramount importance.

In 2003, Tang *et al.* reported the world's first AIE-active polymer and set the stage for many researchers globally to follow this research pathway in understanding the mysteries of the AIE phenomenon.^[20] AIE polymers overall, provides more benefits than small AIE molecules, such as ease of processing, good ability to form films, and structural diversity. Since then AIE polymers have found various applications such as AIE-active polytriazole-based explosive chemosensors synthesized via click polymerization,^[21] high performance polymeric light-emitting diodes with low-cost wet fabrication, high fluorescence quantum nanoparticles with excellent thermal and film-forming stability,^[22] and fluorescent polymeric nanoparticles (FPNs) synthesized from a "one-pot" multicomponent Mannich reaction as bio-imaging agents for L929 cells.^[23] Some reviews have already explored the structure, design, reaction pathways, and applications of AIE polymers,^[16, 18, 24-26] while other reviews explored the area of AIE polymers for biomedical-related applications,^[27] chirality,^[28] supramolecular AIE polymers,^[29] AIE click polymerization,^[30, 31] one-component AIE polymerization, two-component AIE polymerization, and multi-component polymerization.^[30, 32] However, the AIE polymers that were synthesized till date with pre-determined molecular weights, low dispersity values and well-defined structures via Reversible-Deactivation Radical Polymerization (RDRP) specifically has not been systematically summarized. Moreover, these AIE polymers synthesized via RDRP with well-designed structure, chain length, well-controlled molecular weights and molecular weight distributions are of great importance in certain applications such as theranostics, FPNs, and environmental variation detection. Therefore, this review is dedicated to highlight and summarize some of these recent works that utilized RDRP to design and produce AIE polymers, including the different types of RDRP methods, synthetic strategies, and their potential applications.

1.2 RDRP

Since the early 1980s, researchers from around the world have realised that the addition of certain chemical compounds into a polymerization mixture allows reversible reaction with chain carrier molecules.^[33] Many terms have been used to describe these polymerization reactions including (but not limited to): controlled/living radical polymerization, 'controlled' and 'living' polymerization, and radical polymerization with minimal termination'.^[34] In 2010, the International Union of Pure and Applied Chemistry (IUPAC) stepped in to generalize all such polymerization reactions by coining the term: Reversible-Deactivation Radical Polymerization (RDRP).^[33, 34] RDRP can be defined as a polymerization reaction where side reactions such as chain transfer reactions and termination reactions, are considered trivial or negligible throughout the polymerization process and the molecular weight of the growing polymer increases linearly with monomer conversion. This revolutionary polymerization method sparked possibilities in synthesizing complex, well-defined polymer architectures and morphologies with multi-functionalities, which otherwise will not be possible by conventional methods.^[33, 34]

RDRP polymerization techniques include, Nitroxide-Mediated Polymerization (NMP),^[35-37] Atom Transfer Radical Polymerization (ATRP),^[38-45] Reversible Addition-Fragmentation Chain Transfer (RAFT),^[46-49] Iodine-Transfer Polymerization,^[50] Reverse Iodine-Transfer Polymerization (RITP),^[51] Reversible Chain Transfer Catalyzed Polymerization (RTCP),^[52] Reversible Complexation Mediated Polymerization (RCMP),^[53] Organotellurium-Mediated Radical Polymerization (TERP),^[54] Cobalt Mediated Radical Polymerization and Catalytic Chain Transfer (CCT),^[55, 56] Iniferter Polymerization,^[57, 58] Selenium-Centred Radical-Mediated Polymerization,^[59] and Organostibine-Mediated Radical Polymerization (SBRP).^[60] Even though a range of different RDRP technique have been developed over the past decades, the most popular

methods for designing AIE polymers via RDRP are RAFT and ATRP owing to their applicability to a wide range of monomers and reaction conditions, including the robustness of both techniques.

The use of RDRP as a polymerization technique stems from the fact that it is fundamentally more versatile and powerful compared to conventional radical polymerization: (1) the ability to synthesize polymer chains with predetermined molar masses and narrow molar mass distribution (dispersity, M_w/M_n); (2) the ability to continue polymerization by adding more monomers owing to the better stability of the dormant propagating chain; (3) high-chain end fidelity and ease of attaching functional groups to polymer chain ends; (4) lower probability of side reactions such as termination reactions occurring; and (5) ease of fabricating various polymer shapes and morphologies.^[61] All these benefits of using RDRP over other types of polymerization led many researchers to search for and invent unique ways to synthesize polymers with AIE properties in a controlled manner, resulting in a plethora of morphologies discovered and produced over time.

Given the success and advantages of RDRP, this polymerization technique is capable of producing a multitude of polymer morphologies such as single block and block co-polymers spanning a huge range of topological morphologies such as homopolymer, di-/tri-/multi-block, star-shaped, sequence-defined, (hyper)branched, dendritic, graft and brush type, cyclic (ring), network, single-chain nanoparticles (NPs),^[62] bearing unique properties such as stimuli responsiveness to mechanical stress,^[63, 64] temperature and pH changes,^[65, 66] and light irradiation.^[67] Such polymers found potential applications in the field of therapeutics such as nanomedicine, nanotechnology and materials science,^[68-73] energy production and efficiency optimisation, and electronics.^[74-76] Ever since the discovery of the AIE phenomenon in 2001, there are over 10,000 publications till date detailing the different aspects of AIE (**Figure 3**). Specifically, to AIE polymers synthesized using the RDRP techniques aforementioned, there exists more than 140 publications and the number is projected to increase given the multitude of benefits in using RDRP to synthesize AIE polymers. In this review, we describe firstly a brief introduction to RDRP, the AIE phenomenon, and AIE polymers. We will then elaborate on the design of AIE monomers and provide a list of some polymers synthesized via RDRP with the incorporation of AIE moieties. Next, we explore how RAFT can be used to design AIE polymers, including the design, the different types of process and polymerization mechanisms involved. Afterwards, similar to RAFT polymerization, we explore ATRP polymerization. Then, some elaborations on the other types of RDRP for AIE polymers, and potential applications of these AIE polymers. Finally, we present a summary and our perspective on the current progress of the AIE-active polymers.

2. The strategies to incorporate AIE molecules into polymers by RDRP.

By exploiting the versatility of RDRP, AIE molecules can be facilely incorporated into the final polymer product through multiple ways to ultimately synthesize AIE-active polymers; block copolymer containing separate blocks of non-AIE monomers and AIE monomers (**Scheme 1A**), surface-grafted block copolymer (**Scheme 1B**), AIE monomers as crosslinkers for two block copolymers (**Scheme 1C**), AIE moieties as pendent groups in block copolymer (**Scheme 1D**), hyperbranched with random distribution of AIE monomers linked by non-AIE monomer backbone (**Scheme 1E**), four-arm star polymer with AIE moiety as the central core (**Scheme 1F**), end-functionalized AIE moiety chain extended with non-AIE monomers (**Scheme 1G**), direct linkage of AIE monomers (**Scheme 1H**), and unusual AIE behavior of non-AIE monomers after surface-grafted direct linkage (**Scheme 1I**).

Many different combinations of monomers, initiators, linkers, and catalysts type and amount were discovered and experimented to synthesize AIE polymers since the advent of AIE discovery. A few of the more interesting reaction types as examples are listed in **Table 1** that incorporate AIE characteristics into the final polymeric product.

For the reaction types categorized as “RAFT” above, AIBN is typically used as the standard initiator and includes one type of RAFT agent as the chain transfer agent (CTA). Most of the polymerization reactions

listed are considered to be multi-component reactions (MCRs) where more than one type of monomer is involved. For example, **Entry 1 – Entry 4 (Table 1)** involves three different monomers and is considered a random copolymer reaction, where **Entry 4** shows a special case of one of the monomer block (PEG) coupled to the RAFT agent to form a macro-CTA. **Entry 5** and **Entry 6 (Table 1)** are considered a four-component and two-component reaction respectively. **Entry 1 – Entry 6 (Table 1)** are classified as block copolymers containing AIE monomers (**Scheme 1A**). A two-component surface-initiated reaction with the RAFT agent anchored onto a solid surface (**Entry 7, Table 1**) allows for rapid functionalization through surface-grafted block copolymers of non-AIE and AIE monomers (**Scheme 1B**). Further expansion of this concept enabled the successful synthesis of a hyperbranched polymer variant using a non-AIE vinyl-functionalized diamide as a cross-linking backbone (**Entry 8, Table 1**) to incorporate the AIE monomers as pendent groups randomly distributed across the entire polymer molecule (**Scheme 1E**). Functionalization of symmetrical AIE monomers with vinyl bonds imparts cross-linking capabilities in a two-component reaction (**Entry 9 and Entry 10, Table 1**) to crosslink two block copolymers made up of the other non-AIE monomer (**Scheme 1C**). Similar to a hyperbranched polymer mentioned before, the incorporation of an AIE monomer as a pendent group in an MCR (**Entry 11, Table 1**) also endows the block copolymer with AIE properties (**Scheme 1D**).

For all reaction types categorized as “ATRP” above, most of the examples uses AIE molecule-functionalized macro-initiator to produce the final polymeric product possessing AIE characteristics. For example, ATRP initiator core-functionalized with AIE moiety (**Entry 12 and Entry 13, Table 1**) generates four-arm star polymer after polymerizing with non-AIE monomers endows it with unique AIE fluorescence properties (**Scheme 1F**). Another popular choice for incorporating AIE groups into polymers is through end-functionalized AIE moieties (**Entry 14 – 19, Table 1**) with subsequent chain extension using non-AIE monomers (**Scheme 1G**). Polymerizing directly vinyl-functionalized AIE monomers (**Entry 20, Table 1**) provides ease in handling the reaction via direct linkages of the AIE monomers (**Scheme 1H**). Surface-initiated ATRP of AIE-inactive acrylonitrile monomers (**Entry 21, Table 1**) yielded unusual AIE fluorescence behavior in the final product without presence of any phenyl groups or aromatic rings (**Scheme 1I**).

For all reaction types categorized as “Others” above, although Cu(0) polymerizations bear similarities to ATRP, they use different oxidation states of Cu and are considered different to ATRP. Similar to **Entry 1**, AIE monomers are attached to the polymeric product through ionic bonding with *N*-containing non-AIE monomers as backbone (**Entry 22, Table 1**) to form block copolymers with the AIE moieties as pendent groups (**Scheme 1D**). Similar to **Entry 20**, unique designs of AIE monomers are polymerized separately (**Entry 23, Table 1**) through direct linkages (**Scheme 1G**). Similar to **Entry 1 – 6**, complex AIE active monomers functionalized with vinyl bonds (**Entry 24, Table 1**) allows for direct block copolymer synthesis of the AIE monomers separately (**Scheme 1A**). Similar to **Entry 14 – 19**, AIE end-functionalized polymers (**Entry 25 and Entry 26, Table 1**) are produced through polymerizing with non-AIE monomers (**Scheme 1G**).

3. AIE polymers via RAFT

The RAFT polymerization was first reported and invented by Moad, Rizzardo and Thang in 1998 from the Commonwealth Scientific and Industrial Research Organisation (CSIRO) in Australia, as one of the most powerful and versatile polymerization techniques to synthesize uniquely complex polymer architectures.^[46, 47, 77, 78] Coincidentally within a short period of time, Rhodia’s chemists, patented xanthates and coined the term “Macromolecular Design by Interchange of Xanthate” (MADIX).^[79] Due to this coincidence, while both RAFT and MADIX master patents are based off on identical polymerization mechanisms and similarly use thiocarbonylthio compounds (RAFT agents) such as trithiocarbonates, dithioesters, xanthates and dithiocarbamates, the slight difference lies in MADIX only covering xanthates as RAFT agents.^[80]

With over 15,000 papers on RAFT polymerization presently, RAFT is considered technique that emulates

an ideal living polymerization due to its ability to continue polymerization after adding more monomers, has good control over end product polymer molecular weight, generates low dispersity (M_w/M_n) values, excellent tolerance to wide range of monomers bearing functional groups, and the ability to synthesize complex architectures (i.e. brush-shaped, star, hyperbranched, network, etc.)^[62] for various applications such as diagnostic components and biomedical implants,^[81] environmentally-sustainable materials,^[82] and other materials science and medicine-related applications.^[83] Hence, RAFT is suitable for use as a polymerization technique to synthesize AIE polymers.

3.1 RAFT AIE amphiphilic block copolymers

As mentioned in early sections, RAFT allows the preparation of polymers with well-designed structure, well-controlled molecular weights and low dispersity, and these polymer characteristics are critical in the preparation of polymer nano-objects via different types of self-assembly methods, such as solution self-assembly and polymerization-induced self-assembly (PISA). With the more commonly known applications of AIE, the AIE component were also incorporated into block copolymers via RAFT to prepare nano-objects with AIE property for practical applications.

For example, in 2019, Li, Dong and co-workers, used the RAFT technique to synthesize a new class of AIE amphiphilic copolymers, namely, poly(*N*-(2-methacryloyloxyethyl)pyrrolidone)-*b*-poly(lauryl methacrylate-*co*-1-ethenyl-4-(1,2,2-triphenylethenyl) benzene), PNMP-*b*-P(LMA-*co*-TPE) that can self-assemble into various polymer morphologies such as spheres, worms and vesicles in water and *n*-dodecane solvents.^[84] The degree of polymerization (DP) of the PNMP block was kept constant at 35 while varying the P(LMA-*co*-TPE) block. At 1 wt% aqueous solution, spherical micelles of 30-40 nm were formed for PNMP₃₅-*b*-P(LMA₉-*co*-TPE_{0.9}), while worms become dominant for PNMP₃₅-*b*-P(LMA₂₄-*co*-TPE_{2.7}) and PNMP₃₅-*b*-P(LMA₅₅-*co*-TPE_{6.3}). These AIE-active amphiphilic copolymers could act as luminescent probes and were applied in bioimaging using HeLa cells as substrates. Interestingly, quantum yields (QY) of PNMP₃₅-*b*-P(LMA₃₈-*co*-TPE_{4.7}) and PNMP₃₅-*b*-P(LMA₅₅-*co*-TPE_{6.3}) were found to be greatly enhanced compared to others due to higher DP of the AIE-active TPE moiety. Polymer morphology also played a role in enhancing QY where worms were found to increase QY more than spheres. The authors noted that biotoxicity of the polymers increases at higher solid content however, even at a high 40 wt% solid content of PNMP₃₅-*b*-P(LMA₅₅-*co*-TPE_{6.3}), cell viability of HeLa cells is still greater than 85%. This trend was also observed upon increasing copolymer concentration from 10 $\mu\text{g mL}^{-1}$ to 100 $\mu\text{g mL}^{-1}$ at a constant 40 wt% solid content. Under appropriate conditions, these polymers are expected to serve as excellent and highly efficient bioimaging probes.

Variations in the chemical structure of the TPE moiety was also explored by Li and coworkers in 2019 by synthesizing poly(ethylene glycol mono methyl ether)-*b*-poly[(2-(diethylamino)ethyl methacrylate)-*co*-3-(4-(1,2,2-triphenylvinyl)phenoxy)propyl methacrylate)] (PEG-*b*-P(DEAEMA-*co*-TPEMA)) amphiphilic block copolymer where RAFT agent was first coupled to the hydrophilic PEG moiety, with CO₂-responsive PDEAEMA block and AIE active PTPEMA (**Figure 4A**).^[85] The unique reversible transformation process from vesicles to micelles was achieved by reducing the interfacial tension between the hydrophobic blocks and the aqueous solution through adding non-selective co-solvents or upon exposure to CO₂. The reverse transformation from micelles to vesicles can be achieved by bubbling the same solution with argon gas, promoting the release of any encapsulated hydrophilic molecules inside the vesicular compartments, mainly due to the protonation and deprotonation of the DMAEMA block in the polymersomes.

The design of AIE molecules need not be limited to molecules bearing only a single vinyl group, it also applies to molecules bearing two or more of such groups. Zhang, Wei and co-workers in 2013, facilely incorporated a symmetrical cross-linkable AIE dye termed R-E with a vinyl end group on both sides into poly(ethylene glycol mono methyl ether methacrylate) to synthesize R-PEG-20 and R-PEG-40 AIE-based FPNs (**Figure 4B**).^[86] The obtained amphiphilic FPNs is capable of self-assembly in aqueous solution which produces nanoparticles of uniform size, high water dispersibility, strong red fluorescence and excellent biocompatibility, enabling them to serve in cell imaging applications. Cell-counting kit-8 (CCK8) assays were

performed to determine cell viability of these FPNs, and the authors determined excellent cellular uptake levels by A549 cells greater than 90%, even at high concentrations of 80 $\mu\text{g mL}^{-1}$. These FPNs can also be produced from a wide range of monomers and impart greater stability compared to those nanoparticles formed from self-assembly, as FPNs prepared via self-assembly are often unstable in physiological solution due to the weak interactions among these amphiphilic fluorescent molecules. Similar studies have also been conducted by the same group and other groups on preparing AIE dyes via RAFT polymerization capable of self-assembly with similar characteristics since 2014 such as AIE crosslinkers,^[87-94] AIE pendent groups with non-AIE monomers block copolymers,^[95-103] AIE end-functionalized block copolymers,^[48, 49, 104-107] and AIE-functionalized monomers,^[108-119] which helped to expand the library of AIE-functionalized polymers.

Another variation of the commonly known TPE moiety chemical structure was explored by Huang, Liu, Wei and co-workers in 2019,^[120] by combining a novel AIE dye tetraphenylethene-functionalized distyrene (TPES) with poly(ethylene glycol mono methyl ether methacrylate) (PEGMA) to form poly(ethylene glycol mono methyl ether methacrylate)-*b*-poly((*Z*)-3-(4-(1,2,2-triphenylvinyl)phenyl)-2-(4'-vinyl-[1,1'-biphenyl]-4-yl)acrylonitrile)) (PEG-*b*-TS) polymers. PEG-TS1 and PEG-TS2 self-assembled into FPNs with measured diameters of 150 nm and 400 nm respectively in aqueous solutions. Similar to R-PEG-20 and R-PEG-40 reported by Zhang, Wei and co-workers,^[86] PEG-TS series polymers showed greater than 90% cellular viability with HepG2 cells at a concentration of 80 $\mu\text{g mL}^{-1}$.

A less bulky symmetrical TPE-based poly(*N*-isopropylacrylamide-*co*-(*E*)-1,2-diphenyl-1,2-bis(4-((4-vinylbenzyl)oxy)phenyl)ethene) (P(NIPAm-*co*-TPE2St)) was synthesized by Yang, Lin and co-workers in 2022, using thermo-responsive NIPAm blocks and AIE-responsive TPE cross-linking blocks via RAFT technique.^[94] The polymers displayed an emission wavelength of approximately 485 nm and the highest PL intensity when the water fraction reached 90% in a water/THF mixture solvent system. It was also discovered that HepG2 liver cancer cells at a concentration of 2 $\mu\text{g mL}^{-1}$ absorbed over 80% of the polymers. Such polymers can find applications in controlled/target drug delivery, cell imaging and tracking.

In 2017, Liu, Zhang, Wei and co-workers successfully incorporated AIE molecules into polymer particles by combining all multiple reactants together in a multicomponent reaction (MCR) termed the ‘three-component mercaptoacetic acid locking imine (MALI) reaction, with RAFT technique in a “one-pot” reaction to synthesize poly(polyethylene glycol mono methyl ether methacrylate)-*co*-poly(10-undecenal)-poly(((*Z*)-3-(4-aminophenyl)-2-(10-hexadecyl-10H-phenothiazin-3-yl)acrylonitrile) (PPEGMA-*co*-PUCL-Phe1 and PPEGMA-*co*-PUCL-Phe2) (**Figure 4C**).^[121] Luminescent organic nanoparticles (LONs) are capable of self-assembly when dispersed in aqueous medium and are found to possess multiple traits such as AIE features, good brightness, good water dispersibility and excellent biocompatibility. Incubation of HeLa cells with PPEGMA-*co*-PUCL-Phe2 LONs at a concentration of 120 $\mu\text{g mL}^{-1}$ resulted in over 95% cell viability within 24 h, and excellent staining ability at a concentration of 20 $\mu\text{g mL}^{-1}$ believed to be a result of cellular endocytosis.

The incorporation of AIE components into amphiphilic block copolymers enables the preparation of photoluminescent nanoobjects with different morphologies. More recently, with the rising of PISA, AIE-active nanoobjects can be prepared directly during polymerization. As opposed to the previous section on self-assembly, PISA emphasizes on the self-assembly of these morphologies induced/triggered by *in situ* polymerization and not by adding any external agents or stimuli.

For example, in 2017, Wang, Wei, Yuan and co-workers employed the RAFT-PISA process to synthesize poly(*N,N*-dimethylaminoethyl)-*b*-poly[benzyl methacrylate-*co*-1-ethenyl-4-(1,2,2-triphenylethenyl)benzene] (PDMA-*b*-P(BzMA-TPE)) capable of self-assembling into different morphologies such as spheres, worms and vesicles during polymerization (**Figure 5A**).^[122] The authors found that PL intensity and QY increases in the order: PDMA₃₉-P(BzMA-TPE)-120 (micelles) < PDMA₃₉-P(BzMA-TPE)-240 (worms) < PDMA₃₉-P(BzMA-TPE)-360 (vesicles), and that all polymer samples displayed stronger PL intensities when dissolved in water than in ethanol.

Recently in 2022, our group expanded the scope of this area by using the RAFT technique to perform

PISA to synthesize photoluminescent polymer assemblies with rarely-achieved inverse mesophases such as spongosomes, cubosomes and hexosomes (**Figure 5B**).^[123] The resultant polymer PDMA-(PTBA-*r*-PTPE)-CDPA possesses both H₂O₂ responsiveness from the boronic moiety and AIE PL properties from the TPE moiety, allowing the polymer to be stimuli-responsive in addition to luminescence. These higher order morphologies bear high specific surface area and ability to load hydrophilic and hydrophobic chemicals for drug delivery systems and targeted drug release applications.

Similarly, in 2020, Xing and co-workers also realized the unique behavior of DMAEMA when exposed to changes in pH levels and CO₂ presence. They prepared CO₂-responsive polymer morphologies endowed with AIE properties using alcohol RAFT dispersion polymerization to synthesize poly(2-(2-hydroxyethoxy) ethyl methacrylate)-poly(methacryloxyethoxy) benzaldehyde)-poly(2-(dimethylamino)ethyl methacrylate)-poly(4-(1,2,2-triphenylvinyl)phenyl methacrylate) (P(HEO2MA)-*b* - P(MAEBMA-*co* -DMAEMA-*co* -TPEMA)) (**Figure 5C**).^[124] These nano-objects formed via PISA, transformed from spheres to vesicles following an increase in PL intensity. Upon CO₂ bubbling, existing spheres can also transform into a mixture of hemispherical “jellyfish”-like structures and vesicles, while existing vesicles can transform into higher order complex vesicles. The authors also discovered that treatment with CO₂ caused an increase in nano-object sizes from 142 nm to 314 nm (dissolved in methanol) and 146 nm to 358 nm (dissolved in water) over a period of 60 min. A few other similar examples include RAFT-PISA processes in nonsynchronous synthesis of raspberry-like nanoparticles,^[125] in drug delivery systems of where *in situ* drug loading of doxorubicin (DOX) via PISA with azoreductase-responsive PEG-*b* -P(BMA-*co* -TPE-AZO-MMA),^[126] and for *in situ* monitoring and understanding of the photo-PISA process mechanism.^[127]

3.3 AIE block copolymers via Surface-initiated RAFT

AIE molecules can also be polymerized with surface grafted polymers to impart fluorescent properties to the resulting particles via surface-initiated RAFT polymerization. In 2021, Qiao, Pang and co-workers prepared a novel multi-stimuli responsive, multi-functional polymeric nanoparticle poly(2-(dimethylamino)ethyl methacrylate)-*co* -poly((4-vinylphenyl) ethene-1,1,2-triyl)tribenzene) with PDMAEMA as the organic carrier, grafted from SiO₂ surface as the inorganic carrier with asymmetrical encapsulation of Fe₃O₄ nanoparticles (Fe₃O₄@SiO₂@P(DMAEMA-*co* -TPEE)) (**Figure 6A**).^[128] The resulting composite nanoparticle possesses a yolk-shell (YS) morphology with the AIE-active TPEE block, allowing for real-time monitoring of any changes to environmental magnetic field, temperature and pH levels, with the added ability to detect CO₂ presence in aqueous solution. In addition to the commonly known pH/thermo-responsiveness of the PDMAEMA block, the incorporation of Fe₃O₄ endows the polymer with superparamagnetism where higher PL intensity was observed for shorter distance to the source of magnetism. Similar to the works by Li *et al.*^[85] and Xing *et al.*^[124], the authors observed reversible CO₂ detection ability where the PL intensity decreased gradually from pH ~9.5 to pH ~5.5 after bubbling CO₂ for 10 min, and returned to the original pH after bubbling with N₂ gas for the same amount of time. The relative “free” TPE units allowed the polymer brush to respond sensitively and accurately towards these external environmental changes through fluorescence variation. Notably, the solution of YS-NPs exhibited high colloidal stability during the changes, and surface aggregation-induced emission (SAIE) process was proposed for the aggregation of TPE units on the surface of YS-NPs. Another similar study was conducted by Tian, Zhang, Wei and co-workers where fluorescent nanodiamonds (FNDs)-poly(2-methacryloyloxyethyl phosphorylcholine (MPC) (FNDs-polyMPC) composites was fabricated using surface-initiated photoRAFT technique and tested for their high water dispersibility and excellent cellular uptake as cell imaging agents.^[129]

3.4 Hyperbranched AIE block copolymers via RAFT

To prove the versatility of AIE molecules, Bai, Zhang and co-workers in 2018, successfully employed RAFT technique to synthesize a thermo-responsive hyperbranched copoly(bis(*N,N*-ethyl acrylamide))/(*N,N*-methylene bisacrylamide)) (HPEAM-MBA) and copoly(bis(*N,N*-ethyl acrylamide)/4-(2-(4-(allyloxy)phenyl)-1,2-diphenylvinyl)phenol) (HPEAM-TPEAH) polymers (**Figure 6B**) with impressive

Zn^{2+} detection ability as measured directly from fluorescence intensity in the $[\text{Zn}^{2+}]$ range of 4 – 18 $\mu\text{mol L}^{-1}$.^[5] Upon interaction with Zn^{2+} ions, the RIM effect was induced on TPE moieties due to a change in the polymer lower critical solution temperature (LCST) and thereby results in fluorescence, which was considered as a “turn-off” response. The rationale of using Zn^{2+} as opposed to other metal ions such as Na^+ , K^+ , Mg^{2+} , Mn^{2+} , Ca^{2+} , and Fe^{2+} is due to the significant effect on the LCST of the hyperbranched copolymer that Zn^{2+} caused, even at concentrations less than $1 \times 10^{-5} M$. HPEAM-TPEAH also showed greater than 95% cell viability in HeLa cells within 24 h of incubation time for concentration range of $1.0 \times 10^{-6} M$ to $5.0 \times 10^{-5} M$. Another form of hyperbranched polymers is dendritic polymers synthesized by Gao and co-worker in 2013 for the investigation into the cage effect imposed by these polymers on AIE pendent groups, affording the rarely observed solid-state-emissive blue light for such dendrimers.^[130]

4. AIE polymers via ATRP

The ATRP technique was coincidentally invented and discovered separately by three different groups of researchers around the world in 1995: by (1) Sawamoto and co-workers,^[38] (2) Matyjaszewski and co-worker,^[39] and (3) Percec and co-worker.^[40] After ATRP was patented in 1998 by Matyjaszewski and Wang as one of the most successful RDRP process,^[41] numerous other U.S. patents, applications and publications worldwide also featured this polymerization technique.^[43] ATRP is based on a process termed Atom Transfer Radical Addition (ATRA) developed in 1945,^[131] involving the anti-Markonikov addition of alkyl halide radicals to alkenes in the Kharasch addition reactions.^[132] Sawamoto and co-workers in 1995, discovered that by combining ruthenium-based catalyst $\text{RuCl}_2(\text{PPh}_3)$, CCl_4 , and methylaluminum bis-(2,6-di-tert-butylphenoxide) $[\text{MeAl}(\text{ODBP})_2]$ to form a ternary initiating system, it is able to polymerize methyl methacrylate (MMA) via a radical pathway, thus behaving similarly to the ATRA process.^[38] On the other hand, Matyjaszewski and co-workers discovered that polymerising styrene using an alkyl chloride initiator and a $\text{CuCl}/2,2'$ -bipyridine ($\text{Cu}(\text{bpy})\text{Cl}$) catalyst complex yielded well-defined high molecular weight homopolymers with low values.^[39] Later on the same year, Percec and co-worker discovered that styrene polymerisation can also be carried out using arenanesulfonyl chlorides initiators catalysed by CuCl/bpy catalyst complex, producing homopolymers with good conversions but with relatively high values (> 1.50).^[40]

In general, for a typical ATRP mechanism, a redox reaction between an initiator bearing at least one transferable atom(s) or group(s) and a transition metal complex bearing a transition metal salt at a lower oxidation state and ligands attached to it. The metal catalyst cleaves the initiator homolytically and itself is oxidized in the process, enabling monomer addition to take place. The homolytic atom or group then transfers between the growing polymer chain end and the metal catalysts, causing the metal centre to cycle between lower and higher oxidation states, thus establishing a dynamic equilibrium.

ATRP has over 19,000 papers till date covering many areas ranging from synthesis to real-life applications of polymers synthesized from ATRP. ATRP shares the same advantages with RAFT and NMP as it provides a simple route to synthesize polymers with good control of molecular weight, low dispersity (M_w/M_n) values, good tolerance against many functional groups, and the ability to produce well-defined polymer architectures. The main drawback of this technique is the presence of trace amounts of metal ions such as Cu in the end polymer product which is difficult to remove and can pose problems for certain applications. However, this problem can be circumvented by using UV-mediated metal-free catalysts such as the use of phenothiazine^[133] and perylene^{[134], [135]} Nevertheless, the versatility of ATRP enabled it to be used as a technique to synthesize AIE polymers with a slightly different design to the monomers and initiators involved compared to RAFT.

4.1 Core-functionalized polymers AIE polymers via ATRP

A good example of AIE core-functionalized polymer produced via ATRP is by Guan, Lei and co-workers in 2016, where they synthesized a novel polyelectrolyte tetraphenylethene-graft-poly[2-(methacryloyloxy)-ethyltrimethylammonium chloride] (TPE-PMETAC) using ATRP from a TPE-derived four arm macro-

initiator, tetraphenylethylene-2-bromo-2-methylpropionate (TPE-BMP). This polymer is capable of self-assembly into a core-shell microsphere structure in an aqueous solution where the TPE block forms the core and PMETAC forms the shell (**Figure 7A**).^[45] The AIE feature comes from polymer chain aggregation at high concentrations, and is induced by simple exchange of counterions. It was discovered that TPE-PMETAC fluorescence intensity increase nonlinearly with increasing THF volume fraction similar to a phenomenon termed aggregation-induced enhanced emission (AIEE),^[136] giving a bright blue emission at ~ 465 nm in 2/98 v/v water/THF solvent system. In addition, it was observed that the fluorescence intensity of cationic microspheres containing quaternary ammonium groups increases according to the series $\text{Cl}^- < (\text{perchlorate}) \text{ClO}_4^- < (\text{hexafluorophosphate}) \text{PF}_6^- < (\text{bis}-(\text{trifluoromethylsulfonyl})\text{imide}) \text{TFSI}^-$, through ion-pairing interactions leading to “hydrophobic-induced collapse” of PMETAC block.^[45] Reducing the size of microspheres, reduces the electrostatic repulsion forces between each microsphere and induces aggregation, evident in the size of the microspheres ranked from largest to smallest; TFSI^- , PF_6^- , ClO_4^- .

About two years later in 2018, the same group developed persistent fluorescent bioprobes for cell-tracking and identification by synthesizing a novel multi-stimuli-responsive star polymer tetraphenylethene-*graft*-tetra-poly[*N*-[2-(diethylamino)-ethyl]acrylamide] (TPE-tetraPDEAEAM) possessing inherent AIE properties using ATRP technique and TPE-BMP as the macro-ATRP initiator containing AIE-active TPE.^[137] The main difference lies in the stimuli-responsiveness of the side group where the former is electrically charged, while the latter is electrically neutral. These polymers respond to changes in temperature, pH levels and CO_2 levels, with obvious soluble-to-insoluble phase transition at the lower critical solution temperature (LCST). The reversible temperature-responsiveness behavior of TPE-tetraPDEAEAM can be determined by heating it to temperatures above the LCST (turns cloudy) and allowing it to cool down to temperatures below the LCST (reverts back to transparent aqueous solution). In aqueous solution, the LCST decreases from 41.5 to 34.5 °C upon increase of polymer concentration from 0.5 to 2.0 g L⁻¹, along with aggregation of TPE moieties at the LCST of 37.5 °C, resulting in enhanced fluorescence. TPE-tetraPDEAEAM were incubated with HeLa cells for 48 h at a concentration range of 50 – 400 $\mu\text{g mL}^{-1}$ with cell viability of greater than 95%. The polymers are not cytotoxic to the cells at a concentration of 200 $\mu\text{g mL}^{-1}$ for 48 h, which allowed for tracking of the cells for as long as nine passages. Incorporating AIE moieties to functionalize polymer cores were also exemplified by other groups,^[44, 138-144] where they have been used as stimuli-responsive materials, cellular tracking agents, and advanced drug delivery systems.

4.2 End-functionalized AIE polymers via ATRP

End-functionalized polymers with AIE-active moieties can also exhibit fluorescence properties, and was explored by Hadjichristidis and co-worker in 2019.^[145] In this example, the authors synthesized a TPE-terminated linear polyethylene (PE) using Tris(3-(4-(1,2,2-triphenylvinyl)phenoxy)propyl)borane, synthesized from hydroboration of (2-(4(allyloxy)phenyl)ethene-1,1,2-triyl)tribenzene with BH_3 , as an initiator for the polyhomologation of dimethylsulfoxonium methylide to afford well-defined *a*-TPE- ω -OH linear polyethylenes (PE). All polymeric products showed AIE fluorescence either in the bulk phase or the solution phase, due to self-assembly behavior of the PE-based block copolymers in DMF solvent. The fluorescence intensity of the solutions can be determined from the block copolymer compositions and micelle size. At 90% v/v *n*-hexane fraction in a 0.1 g L⁻¹ toluene/*n*-hexane solvent system, the highest PL intensity was observed which is 4.5-fold higher than pure toluene solvent system. For TPE-PE-*b*-*Pt* BuA polymers, the critical micelle concentration (CMC) values are in the range of 0.5 – 1.5×10^{-2} mg mL⁻¹, with the highest CMC value recorded to be 1.47×10^{-2} mg mL⁻¹ for the polymer with the highest *Pt* BA content. The authors then extended their work to synthesize amphiphilic block copolymers TPE-PE-*b*-PAA by treating TPE-PE-*b*-*Pt* BA with TFA to hydrolyze the *t* Bu group to COOH group.^[146] The synthesized polymer is responsive to pH changes and it can emit fluorescence when exposed to certain ions. Changes in fluorescence intensity was attributed to pH responsivity of the PAA block, causing different degree of aggregation of the TPE block. In addition, the influence of different cations at different pH levels on the fluorescence of TPE-PE-*b*-PAA was also investigated. The authors found that for the cations; Li^+ , Na^+ , K^+ , Cs^+ , electron cloud polarizability was the dominant factor in determining fluorescence intensity, and therefore ranked them in

increasing fluorescence order $\text{Li}^+ < \text{Na}^+ < \text{K}^+$. Cs^+ has the largest polarisable electron cloud, however due to the secondary factor electron repulsion, it was not ranked after K^+ .

PhotoATRP can also be a viable option to synthesize polymers, which was exploited by Yang, Xiao and co-workers in 2021, to produce poly(methyl methacrylate)s (TPE-PMMA) with AIE properties by combining methyl methacrylate monomers with 4-(1,2,2-triphenylvinyl)benzyl 2-bromo-2-phenylacetate (TPE-BPA) AIE-functionalized initiator, and catalyzed by air-stable copper(II) bromide/tris(2-pyridylmethyl)amine ($\text{Cu}^{\text{II}}\text{Br}_2/\text{TPMA}$) photocatalyst under benign conditions.^[147] Polymerization reaction was conducted using LED light of wavelength 405 nm, and the introduction of the TPE moiety did not affect the polymerization kinetics and temporal control. AIEE effect was observed for TPE-PMMA solutions with higher molecular weights and with increased viscosity.

In 2016, Hong and co-workers prepared AIE-active amphiphilic tetraphenylthiophene (TP)-terminated poly(acrylic acid) (TP-PAA) using ATRP technique.^[148] The resulting polymer self-assembled, primarily through hydrogen bond among carboxylic acid moieties at concentrations above the critical aggregation concentration (CAC) to form aggregates. The *t* BA pendant groups can be hydrolyzed by acids to the final AA pendant groups. In water, when TP-PAA concentration exceeds the CAC value (5.25×10^{-6} M), the polymers aggregate into small micelles and fluoresces. At pH 2 to 9, there is almost negligible fluorescence as the fraction of aggregate emission is less than monomer emission. In contrast, at pH 9 to 12, the polymer fluoresces strongly. The authors tested TP-PAA as a potential bovine serum albumin (BSA) detector, where aggregate emission was more pronounced when mixed with BSA than the monomer emission.

Expanding on the application aspect of AIE-active polymers, in 2018, Liu, Li and co-workers prepared polymeric micelles based on tetraphenylethene (TPE) conjugated poly(*N*-6-carbobenzyloxy-L-lysine)-*b*-poly(2-methacryloyloxyethyl phosphorylcholine) (TPE-PLys-*b*-PMPC) copolymer, which contains AIE-active TPE block in the micelle core (**Figure 7B**).^[149] The polymers were then loaded with an anti-cancer drug, DOX, for triggered intracellular drug release traced by fluorescent imaging of the micelles, which was made possible through hydrophobic interaction between DOX and PLys blocks in the polymer. Blank TPE-PLys-*b*-PMPC showed insignificant toxicity while DOX-loaded micelles showed excellent growth inhibition against HeLa cells and 4T1 cells, making such polymers a good candidate for antitumor and anticancer treatments.

Variations in the chemical structure of the AIE moiety, besides the commonly known TPE functional group, can also be employed to expand the range of choice of AIE molecules. Ouyang, Zhang, Wei and co-workers in 2020, prepared AIE-active FPNs 10-phenylphenothiazine-poly(benzyl methacrylate-*co*-2-methacryloyloxyethyl phosphorylcholine) (PTH-P(BzMA-MPC)-20(40)) capable of self-assembly into spherical micelles (**Figure 7C**).^[150] PTH-P(BzMA-MPC)-20 with ratio of PTH-Br/MPC/BzMA as 1/40/20 and PTH-P(BzMA-MPC)-40 with ratio of PTH-Br/MPC/BzMA as 1/40/40 FPNs emit fluorescence intensely with high quantum yield of 34.3% and 41.2% respectively measured against Rhodamine B (1 mg/mL) in ethanol as the standard, good water dispersibility and low CMC values. PTH-P(BzMA-MPC)-20 and PTH-P(BzMA-MPC)-40 FPNs were evaluated for cell viability with L02 cells, with both polymers bearing greater than 90% cell viability even after 24 h incubation at a concentration of 320 $\mu\text{g/mL}$.

In 2012, Xu, Lu and co-workers synthesized a pyrazoline-based TPP-NI possessing a electron donor group (dimethyl-amino) and an electron acceptor group (1,8-naphthalimide) capable of intramolecular charge transfer (ICT) and AIE effects. TPP-NI was then used as the initiator to polymerize styrene (St), methyl methacrylate (MMA), and 2-hydroxyethyl methacrylate (HEMA) separately.^[151] With reference to the PL intensity of pure DMF solution, PS showed 155-fold increase in PL intensity when dissolved in DMF-ethanol solvent system, while PMMA showed 65-fold increase when dissolved in DMF-water system, and PHEMA showed 10-fold increase when dissolved in DMF-water system with 70-fold increase when the solvent was acidified. PHEMA amplifies the pH value effect as it causes more dimethylamino groups of TPP-NI to be exposed, which made it possible for PHEMA to serve as an optical sensor and drug-delivery agent via effective encasement of hydrophobic drug molecules. In a few other similar examples, AIE end-functionalized polymers were also synthesized,^[152-156] where they have been used to study the ATRP process mechanism and certain stimuli-responsive polymers for material fabrications.

4.3 AIE monomer/component-functionalized polymers via ATRP

Xu, Lu and co-workers have explored the possibility of transforming the ICT, AIE dual property molecule into a polymerizable monomer in 2013, and successfully synthesized poly(2-butyl-6-(5-(4-(diethylamino)phenyl)-3-(4-(4-vinylbenzyloxy)phenyl)-4,5-dihydro-1*H*-pyrazol-yl)-1*H*-benzo-*[de]*isoquinoline-1,3(2*H*)-dione) (PStTPP-NI) using ATRP technique.^[157] The fluorophore displays AIEE effect and increased quantum yields in strong polar solvents. StTPP-NI shows almost negligible QY in DMF solution (0.16%), while bearing a high QY of 27% in cyclohexane solution. In another example where Luo, Li and co-workers in 2020, synthesized P(*t*BA-*r*-TPEA)-*b*-PCholMA) (**BCP-1**) from acrylate-functionalized TPE units (TPEA), where these AIE-active units are found in the corona forming part of the block copolymer.^[158] Quantum yield after micellization of **BCP-1** was found to greatly increase from 0.38% (before micellization) to 9.36%, which can be used to monitor the micellization process and to study the effects of solvents on the process. Furthermore, some variations of AIE-functionalized components include AIE moieties as pendent groups,^[159] as monomers,^[160, 161] and as part of hyperbranched polymers,^[162] were exemplified by other groups using ATRP.

4.4 AIE polymers via Surface-initiated ATRP

Surface-initiation methods imparts different unique properties onto the solid surface and enables good customization of these surfaces. In 2017, Wen, Zhang, Wei and co-workers incorporated AIE functionalities onto silica nanoparticles (SNPs) via the Stöber method to prepare luminescent silica nanoparticles (LSNPs), which was then converted into a macro-initiator where zwitterionic 2-(methacryloyloxy)ethyl phosphorylcholine (MPC) monomers were polymerized via surface-initiated ATRP (SI-ATRP) to form SNPs-AIE-pMPC (**Figure 8A**).^[163] Similar to the work by Ouyang, Zhang, Wei and co-workers in 2020,^[150] Xu, Zhang, Wei and co-workers had extended their work from randomly dispersed PTH-P(BzMA-MPC)-20(40) FPNs to PTH-functionalized mesoporous silica nanoparticles (MSNs) with surface grafted block copolymer PTH@MSNs-poly(PEGMA-*co*-IA) from poly(ethylene glycol)methyl acrylate (PEGMA) and itaconic acid (IA) as monomers using light irradiation.^[164] Some interesting properties of this polymer includes the ability to conjugate with the anticancer drug *cis*-diammineplatinum dichloride (CDDP) with pH-responsive behaviors for sophisticated controlled drug delivery systems with high water dispersibility, low cytotoxicity and excellent candidate as a cell imaging agent.

The scope of AIE molecules can also be expanded to include molecules with no perceivable aromatic rings or AIE-like features. An unusual case of AIE fluorescence was reported by Kopeć and co-workers in 2020, when ATRP was used to synthesize and graft well-defined low molecular weight ($M_n < 10,000 \text{ g mol}^{-1}$) polyacrylonitrile (PAN) from silicon (Si) wafers (**Figure 8B**).^[165] PAN is a non-conjugated polymer that does not contain any phenyl ring structures, yet it is still capable of AIE fluorescence behavior. The reason can be explained by the clustering of the nitrile groups in PAN, causing an overlap of π and lone pair electron clouds, resulting in similar RIM effects as TPE groups.^[166] These PAN brushes were prepared via photoinduced ATRP, allowing for significant reduction in catalyst amounts. A review put together by Yuan and Zhang in 2016,^[167] elaborates in more detail the beauty of nonconventional macromolecular luminogens with AIE characteristics which can be attributed to the similar clustering behavior as PAN, resulting to fluorescence of the polymeric product.

5. AIE polymers via other RDRP methods

Of the many types of RDRP, Cu(0)-RDRP and NMP were the other methods to synthesize AIE polymers. Cu(0)-RDRP was first reported by Matyjaszewski, and co-workers in 1997 when they discovered that the addition of zerovalent copper metal powder into standard ATRP polymerizations of styrene and (meth)acrylates dramatically improved the rate of reaction by as much as 10-fold compared to without any addition of the powder via simple electron transfer process to remove excess Cu(II) deactivator species.^[168] In

2006, Percec, Sahoo and co-workers termed this unique polymerization technique as Single-Electron Transfer Living Radical Polymerization (SET-LRP),^[169] which helped differentiated it from the standard ATRP technique.

NMP was first reported and patented by Solomon, Rizzardo and Cacioli of CSIRO Australia in 1986.^[35] Similar to RAFT and ATRP, NMP is a technique that bears resemblance to an ideal living polymerization: (1) the ability to control desired polymer product molecular weight with low dispersity (M_w/M_n) values, (2) has realistic industrial potential with simple implementation steps that often requires only a single unimolecular initiator to produce the desired product, and (3) no need for use of transition metal catalysts. NMP uses alkoxyamine initiators which can undergo homolysis of the C-O bond to yield a stable nitroxide radical that is characteristic of a persistent radical, leading to favoured generation of one product over all others.^[170-173] Given the benefits Cu(0)-RDRP and NMP can offer, they are considered suitable methods for synthesizing AIE polymers.

In 2021, Haddleton, Zhang and co-workers synthesized cationic glycopolymers structurally similar to poly(ionic liquids) (PILs) using Cu(0)-RDRP technique.^[174] Post polymerization modifications were performed on the poly(4-vinyl pyridine) (P4VP) groups with halogen-functionalized D-mannose and TPE units, thus imparting AIE properties onto the resulting polymer. The resulting polymer can be viewed as cationic glycopolymers which is a hybrid material possessing both PIL and glycopolymer properties, which includes specific carbohydrate-protein recognition and antibacterial activities in bacteria such as Gram-positive *Staphylococcus aureus* and Gram-negative *Escherichia coli*. The TPE units have the ability to improve the interaction between PILs and bacteria surface biomacromolecules, causing further aggregation of PILs and concentration of TPE units in the bacteria leading to AIE fluorescence for fluorescence imaging. The combination of AIE-active TPE units with glycopolymers and PILs enables the tracking, killing and detection of bacteria. For the synthesis of PILs, Cu(0)-RDRP was used to polymerize 4VP to obtain P4VP at high conversion of 94% at room temperature conditions in DMSO:H₂O solvent system (v/v = 1:1). Then, quaternization reaction was employed to modify P4VP with organobromides such as TPEBr, Mannose-Br, or 2-bromopropanol, yielding PILs of P4VP-ManTPE and P4VP-BPTPE. The PILs adsorbs onto the bacteria surface via electrostatic interactions between positively-charged pyridine rings and negatively charged bacterial membranes, while the hydrophilic parts may insert into the hydrophobic membrane parts to kill the bacteria. The authors noted that cationic glycopolymers have better bactericidal effects on Gram-positive bacteria than Gram-negative bacteria due to the difference in cell membrane structures. Concanavalin A was used to show that sugar-containing PILs can recognize proteins, leading to aggregation and significant AIE effect. It is also worthwhile to note, detection by fluorescence emission of bacteria became more sensitive when bacteria concentration increases due to the AIE effect.

Similar to RAFT and ATRP, Cu(0)-RDRP need not be limited to the commonly known AIE-active TPE molecule, other variations were explored by many research groups, for example, Hudson and co-workers in 2018, prepared three different acrylic monomers using organic semiconductors as motifs, and employed them as electron-transporting (n-type) materials.^[175] Cu(0)-RDRP method was used to prepare triazine-, oxadiazole-, and benzimidazole- containing polymers from room-temperature reaction using Cu(0) wires to give low dispersity ($\text{M}_w/\text{M}_n = 1.14$) and high conversions of up to 97%. The authors faced a problem with benzimidazole-containing monomers due to the large induction period prior to onset of polymerization attributed to slow coordination of benzimidazole groups to CuBr₂. Due to the limited solubility of these hydrophobic monomers in polar solvents such as DMSO, DMF and isopropanol, difficulties were faced when selecting appropriate solvents. *N*-methyl-2-pyrrolidone and *N,N*-dimethylacetamide (DMAc) solvents were found to be effective in dissolving the monomers and assisting in the catalysts activities. Higher molecular weights of the resulting polymers were also successfully achieved at a lower conversion percentage and broader M_w/M_n , which could be due to poorer overall polymer solubility. Nevertheless, Cu(0)-RDRP was successfully employed by the authors to synthesize polymers with optical properties from challenging monomers containing *N*-donor groups with low dispersity values ($\text{M}_w/\text{M}_n = 1.14 - 1.39$) and conversions higher than 92%. All polymers were found to be thermally stable, as determined from only a single step decomposition at 275 °C, making them ideal for processing into organic devices such as organic light-emitting diodes (OLEDs),^[176] organic photovoltaics

(OPVs),^[177] organic thin-film transistors (OTFTs),^[178] organic electrochemical transistors (OECTs) and organic thermoelectric (OTE) generators.^[179]

AIE molecules can also include transition metals such as iridium (Ir) which allows tuning of the color of fluorescence emitted. In 2019, Hudson and co-workers synthesized a series of bottlebrush copolymers (BBCPs) from red (IrPIQ-MM), green (IrPPY-MM), and blue (tBuODA-MM) (RGB) luminescent macromonomers using a carbazole-based host, which was then used to prepare multiblock organic fibres with similar structures to nanoscale RGB pixels (**Figure 9A**).^[180] The different blocks were then combined to give di- and tri-block luminescent BBCPs, which displays AIE effects between blocks as the solvent polarity changes. The authors elaborated on solvent-responsive luminescent encoded patterns by quantifying the changes in energy transfer efficiency and interchromophore distance among the different blocks after aggregation. White LED mimicking pentablock nanofibers were then synthesized containing multiple discrete emission zones by combining the different building blocks with charge-transporting materials. Well-defined interfaces in BBCPs can be used to regulate energy transfer between the segments. Forster resonance energy transfer (FRET) were observed with significant color change when BBCPs aggregate. Multicomponent nanofibers with increasing complexity can be prepared using this method to conduct studies on optoelectronic interaction between and within BBCPs.

An initiator containing a norbornene moiety and a carbazole-based acrylic monomer (CzBA) were used to copolymerize with 8 wt% of different luminescent material, yielding materials with tunable colors via Cu(0)-RDRP. In this study, acrylic-based monomers containing Ir(piq)₂(acac), Ir(ppy)₂(acac), (piq = 2-phenylisoquinoline, ppy = 2-phenylpyridine) (IrPIQ and IrPPY), and donor-acceptor type monomer 4-(5-([1,1'-biphenyl]-4-yl)-1,3,4-oxadiazol-2-yl)-*N,N*-di-*p*-tolylaniline (tBuODA) were employed to produce polymers that emit red, green, and blue light respectively. *Grafting through* approach was used to give tBuODA_{75-b}-IrPPY_{75-BB}, tBuODA_{60-b}-IrPIQ_{90-BB}, and IrPPY_{100-b}-IrPIQ_{50-BB} diblock copolymers in a way that emits colors intermediate to both constituent homopolymers. Well-defined two-color interface was observed upon combining the chromophores with a BBCP controllable solvent polarity. As the water fraction increases from 0 to 98% in the solution of tBuODA_{75-b}-IrPPY_{75-BB}, tBuODA_{60-b}-IrPIQ_{90-BB}, phosphorescence was observed to increase significantly for the red and green iridium fluorophores, while blue fluorescence decreases gradually. Due to significant spectral overlap between tBuODA and IrPPY emission profiles, energy transfer efficiency for tBuODA_{75-b}-IrPPY_{75-BB} could not be accurately determined. In addition, BBCPs can be used to prepare nanofibers with multiple compartments. A linear “pentablock” nanofiber mimicking a white OLED design with discrete RGB emissions was prepared, possessing unique characteristics such as high energy efficiency and diffuse lighting for use as a potential next-generation solid state lighting.

In addition, Cu(0)-RDRP can be employed to synthesize polymers capable of behaving as drug carriers as exemplified by Jia, Tang and co-workers of which they synthesized a brush-like polymer with AIE features for drug delivery and intracellular drug tracking.^[181] The study aims to improve the loading capacity of drug carriers by using a brush-like polymer with many functional groups capable of holding the target drug compound. By combining TPE bromoisobutyrate (TPEBIB) and anticancer drug doxorubicin (DOX),^[182] it could potentially lead to a compound capable of real-time monitoring of cell targeting, drug release and cancer cell viability. TPEBIB was synthesized and used as an initiator in the copolymerization of poly(ethylene glycol) acrylate (PEGA) and hydrazine (Hyd) monomers via Cu(0)-RDRP, and subsequently conjugating DOX to the centre carrier through the hydrazone bonds to form the complex carrier TPE-PEGA-Hyd-DOX smart prodrug containing approximately 11 wt% DOX.^[181] DOX is released in a controlled manner when exposed to cancer cells due to hydrazine bond cleavage in acidic conditions due to improved cellular uptake levels. This novel block copolymer is completely biocompatible with normal and cancer cells, with the cytotoxicity depending on the local pH levels. A comparison study was performed between pristine DOX solution as the control and TPE-PEGA-Hyd-DOX solutions at the same concentration, where drug release reached only 10% after 96 hours under normal cell conditions compared with 40% after 24 hours under cancer cell conditions helps confirmed that conjugation of DOX to the drug carrier controls the release of DOX and protects normal cells against DOX. Many other studies also employed the Cu(0)-RDRP methods to synthesize AIE polymers such as Cu(0)-catalyzed SET-LRP reported by Wang, Yang

and co-workers for the study of multi-arm star polymers with TPE-functionalized core,^[183] and the study of through-space charge-transfer thermally activated delayed fluorescence (TSCT-TADF) phenomenon using AIE-functionalized monomers.^[184-186]

NMP can also be used for the synthesis of AIE polymers with a unique morphology as demonstrated by Nicolas and co-workers in 2017, whom employed carbodiimide chemistry to link 4-(*N*-methylpiperazine)-1,8-naphthalimide-based AIE dye,^[187] with AMA-SG1 alkoxyamine, yielding Napht-AMA-SG1 in 82% yield via the *grafting from* or ‘drug-initiated’ method. Isoprene monomers were then added to produce the AIE-active polymer 4-(*N*-methylpiperazine)-1,8-naphthalimide-polyisoprene (Napht-PI) and subsequently, co-nanoprecipitated with cladribine-diglycolate-polyisoprene (CdA-digly-PI) to form Napht-PI CdA-digly-PI prodrug nanoparticles (**Figure 9B**).^[188] Cytotoxicity of the polymers synthesized were also determined by incubating with murine leukemia (L12210) cells, with cell viability reaching approximately 100%, up to a concentration of 250 $\mu\text{g mL}^{-1}$ after 72 incubation time. Confocal laser scanning spectroscopy (CLSM) on Napht-PI CdA-digly-PI prodrug nanoparticles were carried out through incubation with A549 human lung carcinoma cells for intracellular imaging. The low cytotoxicity of these nanoparticles combined with the sharp fluorescence signal from the AIE-active part of the prodrug, provides excellent imaging and tracking abilities in living cells. It is worth noting that the 1,8-naphthalimide-based fluorescent dyes studied in Nicolas’ work,^[188] were used previously to conjugate with different chemical species due to their versatile chemical structures.^[189] These dyes exhibit AIE properties due to a twisted intramolecular charge transfer (TICT) process originating from RIM.

The use NMP in AIE polymer synthesis was also demonstrated by Qiao, Pang and co-workers in 2021 where TPE-functionalized 4-amino-2,2,6,6-tetramethylpiperidine-1-oxyl (NH_2 -TEMPO) and 3-(((2-cyanopropan-2-yl)oxy)(cyclohexyl)amino)-2,2-dimethyl-3-phenylpropanenitrile (Dispolreg 007) were used to study reaction kinetics in homogenous and heterogenous polymerization systems respectively.^[37]

6. Applications of AIE polymers.

AIE polymers have various applications ranging from using them as tools in studying reaction mechanisms to different types of sensors to theranostic applications, and so on.^[4, 12, 190-193] In this section, some examples will be highlighted with more emphasis on theranostic applications, which briefly describes the importance of AIE polymers and how AIE polymers can improve our daily activities.

6.1 Theranostics

Theranostics is a novel concept which combines diagnosis (cell imaging) and therapy treatment (targeted drug release) in a full drug delivery system where AIE polymers are utilized as drug trackers to monitor the release of drug molecules after entering the targeted cells. Biological imaging techniques have played an important role in the field of biomedical application such as in guiding drug carriers for targeted cell treatments, cancer cell detection and stem cell transplantation. Fluorescence imaging garnered worldwide interest as the “next-generation” technology in high precision imaging at the subcellular level, with strong PL, high sensitivity and versatility in the designing of the fluorescent nanoparticles.

Zhang, Wei and co-workers reported red R-PEG series and red R-F127 series fluorescent organic nanoparticles (FONs) in 2013 and 2014 respectively,^[86, 194] with excellent cell compatibility of at least 90% against A549 cells. Ouyang, Zhang, Wei and co-workers in 2020, reported the facile preparation of AIE-active PTH-P(BzMA-MPC) FPNs with good water dispersibility and similar cell compatibility percentage against L02 cells as the previously mentioned FONs.^[150] Similar trend patterns in cell penetration ability of both types of FONs and FPNs were confirmed by Confocal Laser Scanning Spectroscopy (CLSM).

Drug delivery systems containing self-guiding carrier molecules for anti-cancer drug treatment became popular in recent years. The use of anti-cancer drugs alone led to an increased possibility of drug resistance

development in cancer cells,^[195] and the lack of real-time monitoring of the entire delivery system of drug contributed to the limited application in cancer cell treatments. In 2018, Liu, Li and co-workers prepared poly(*N*-6-carbobenzyloxy-L-lysine)-*b*-poly(2-methacryloyloxyethyl phosphorylcholine) (TPE-PLys-*b*-PMPC) capable of spherical core-shell self-assembly with encapsulation of DOX in the micelle core via hydrophobic interactions for intracellular release and tracking (**Figure 10A**).^[149] CLSM images were taken after incubating DOX-loaded TPE-PLys-*b*-PMPC with HeLa cells, where the images are taken at timestamps of 2, 4, 6, and 8 h. Red fluorescence pattern trends revealed that DOX entered the cytoplasm during the first 4 h after incubation, and slowly diffuses into the cell nuclei from the 6 h mark onwards, while blue fluorescence pattern trends suggests that TPE-PLys-*b*-PMPC remains only in the cell cytoplasm. TPE-PLys-*b*-PMPC improves the endocytosis of DOX and degrades during the first 4 h after incubation through which DOX was released, that will ultimately diffuse into the cell nuclei and inhibit cancer cell growth. This mode of mechanism is one of the ways for designing smart drug delivery systems with triggered biodegradable drug carriers.

Based on similar principles of intracellular drug release, Jia, Tang and co-workers in 2022 synthesized TPE-PEGA-Hyd-DOX with a slightly different drug release mechanism, where the hydrazone bond acts as the linker and conjugated with the anti-cancer drug DOX.^[181] Confocal images of TPE-PEGA-Hyd-DOX, TPE-PEGA-Hyd, and pristine DOX were taken after incubation with HeLa cells and NIH3T3 cells respectively with a much stronger fluorescence registered for TPE-PEGA-Hyd-DOX in both cases. The DOX channel image represents the extent of release of the drug into the cells. In both cases, pristine DOX uptake was relatively less readily than TPE-PEGA-Hyd-DOX, where the merged images confirmed the excellent performance of this drug carrier delivery system. In addition, Jia, Tang and co-workers found that drug release was limited in healthy cells compared to cancer cells as the environment in the cancer cells encouraged the hydrazone bond cleavage and subsequent release of DOX in the cell cytoplasm, where it migrated into the cell nuclei to kill the cells. The combined benefits of AIE and targeted drug delivery enabled this drug delivery system to monitor drug movement and *in vivo* cellular responses in real-time which can help to revolutionise traditional methods in direct administration of medicinal drugs.

In another work by Liu, Tang and co-workers in 2012, TPE-functionalized 2-(2,6-bis((*E*)-4-(phenyl(4'-(1,2,2-triphenylvinyl)-[1,1'-biphenyl]-4-yl)amino)styryl)-4*H*-pyran-4-ylidene) malononitrile (TPE-TPA-DCM) with strong PL intensity in the far-red/near-infrared (FR/NIR) electromagnetic region, was combined with BSA as the polymer matrix to form uniformly-sized protein nanoparticles (**Figure 10B**).^[190] These FPNs were then examined for their cell compatibilities against MCF-7 breast cancer cells and murine hepatoma-22 (H₂₂)-tumor-bearing mouse models. *In vivo* imaging of BSA-loaded FPNs were determined via non-invasive fluorescence imaging of the live animals after injection of the FPNs with images taken at the 3 h, 8 h, 28 h mark for BSA-loaded FPNs and bare FPNs respectively, where fluorescence intensity was twice as high for the mice with tumors than for the mice without any tumors. *Ex vivo* imaging on the different parts of the mice when it was sacrificed 24 h post-injection helps to confirm the accumulation of the BSA-loaded FPNs in the tumor areas through visualization of the intense coloration in that particular area.

6.2 pH level fluctuation sensor

By incorporating stimuli-responsiveness into AIE polymers, it can respond to environmental variations such as temperature, light, pH and many more. One of the important modifications performed to AIE polymers is the ability to detect environmental pH changes, which becomes important when dealing with biological applications such as intracellular drug delivery and carrier systems.^[196]

Recently, a study was conducted by Li, Sun and co-workers in 2021, where block copolymer poly(ethylene glycol)-*b*-poly(L-lysine) (PEG-*b*-PLys) was synthesized and modified with TPE-CHO group to form PEG-*b*-P(Lys-TPE) bearing reversible pH-responsive fluorescence properties.^[4] PEG-*b*-P(Lys-TPE) forms spheres with a core-shell structure when added to a solvent system comprising DMF/H₂O, and forms vesicles when added to a solvent system comprising THF/H₂O. For the THF/H₂O solvent system, fluorescence intensity dropped drastically upon reducing pH level from 10.7 to 1.4, postulated to be the detaching of the TPE

moiety from the imine bond, causing the polymer to lose the AIE characteristics, while regaining strong fluorescence after increasing the pH level to 12.6, indicating the re-attachment of the TPE moiety to the polymer via the imine bond (**Figure 10C**). The authors also found that this reversible behavior is only possible in a mixed solvent system as the polymer exhibited irreversible pH fluorescence behavior when pH variations were performed in pure water solvent systems due to the precipitation of TPE residues after detachment from the polymer. Nevertheless, such a polymer can find potential use as a pH probe in mixed solvent systems but has limited applications in single solvent systems.

6.3 Metal ion selective sensor

Metal ion pollution is a major environmental concern and it is crucial that these metal ion can be readily detected through the use of probes that interact with them and provide sensing capabilities. Fluorogenic probes have the ability to interact with the metal ions via complexation and other chemical reactions to change their fluorescence properties, which can be detected by fluorescence measurements.^[197] AIE-based polymer probes can be designed to take advantage of the metal ion-induced aggregation effect to detect a single type or multiple types of metal ions by registering a change in fluorescence intensity.

Metal ion probes can also be designed to detect a single type of metal ion instead of multiple metal ions. Bai, Zhang and co-workers in 2018, facilely constructed a hyperbranched AIE poly(acrylamide) HPEAM-TPEAH to be used as a probe for the detection of Zn^{2+} specifically.^[5] An aqueous mixture of fluorescence HPEAM-TPEAH and different metal ions were prepared to determine which metal ion is responsive towards HPEAM-TPEA, and the authors discovered amongst the many metal ions tested such as Zn^{2+} , Mn^{2+} , Na^+ , Ca^{2+} , Mg^{2+} , Fe^{2+} and K^+ , only Zn^{2+} ion provided a significant decrease in fluorescence intensity when mixed with HPEAM-TPEAH in water and in simulated body fluid. Zn^{2+} ion remained detectable even at low concentration of $2 \times 10^{-5} M$, indicating the highly selective and sensitive “turn-off” response of HPEAM-TPEAH towards Zn^{2+} ion.

7. Summary and perspective.

This review summarizes some of the many interesting AIE polymer end product design from a wide range of monomers and some important applications that AIE polymers can bring about. The unique discovery of the AIE phenomenon manages to solve problems associated with the ACQ phenomenon as aggregation is highly encouraged for AIE polymers to be useful. Due to the versatility of RDRP, various strategies can be used to incorporate AIE components into polymers such as direct polymerization of non-AIE monomers and AIE monomers, surface-initiated polymerization, AIE monomers containing more than one vinyl bond acting as crosslinkers, AIE components as pendent groups which can be found in hyperbranched-type polymers, AIE core-functionalized multi-arm star polymers, AIE end-functionalized polymers, direct linkage of AIE monomers, and through the unusual AIE fluorescence behavior exhibited after polymerizing non-AIE monomers. More efforts are being invested in discovering other possible combinations of monomers and initiators/crosslinkers to produce unique AIE polymers possessing multi stimuli-responsive properties for high-throughput new applications or improving upon currently known applications including their use as cell imaging agents and drug delivery systems in theranostics applications, pH sensors, and metal ion selective sensors. An emerging trend in the AIE polymer field is the shift towards simpler fabrication processes where multicomponent reactions and one-pot reactions assisted by microwave or ultrasonic irradiation are favoured over tedious multi-step preparations. Another exciting area of AIE polymers is the use of carbohydrate-based monomers and unusual monomers without phenyl groups but still able to possess AIE characteristics after polymerization such as acrylonitrile, and epoxide-containing branched monomers, which may find application for imaging and biological related purposes.

The possibility to combine artificial intelligence (AI) and machine learning (ML) to AIE polymers fabrication and application opens up exciting future directions for high-end technologies such as incorporation of AIE polymers into AI systems with complex logic gates as multi-sensors, advanced ML models that can rapidly

predict structure-property relationships (SPRs) of AIE/ACQ polymers, ML tools with the ability to generate fast and accurate information on pathogens through AIE responsiveness to environmental variations, and so on. In addition, AI and ML can also be applied to automate polymerization techniques on the benchtop to quickly screen and identify different SPRs in a large chemical space for high throughput experiments and high throughput screening, which would otherwise require laborious work by researchers. Even though AIE polymers became popular more than a decade ago, it can only be considered in the infancy stage of development as many of the applications are being constantly developed and improved upon. With the unwavering efforts of many researchers around the world, AIE polymers will become even better and more useful in the future.

Acknowledgements

The authors acknowledge funding support from the Australian Research Council for the ARC Centre of Excellence for Enabling Eco-Efficient Beneficiation of Minerals (Grant No. CE200100009). N.K.S.T. would like to thank the scholarship offered by the Monash University. The authors gratefully thank Dr Heather F. Cole for help with the SciFinder^m literature search.

Conflict of Interests

The authors declare no conflict of interests.

8. References:

- [1] A. A. Nagarkar, S. E. Root, M. J. Fink, A. S. Ten, B. J. Cafferty, D. S. Richardson, M. Mrksich, G. M. Whitesides, *ACS Cent. Sci.* **2021** , 7 , 1728-1735.
- [2] M. Zimmer, *Chem. Rev.* **2002** , 102 , 759–782.
- [3] E. Wang, E. Zhao, Y. Hong, J. W. Y. Lam, B. Z. Tang, *J. Mater. Chem. B.* **2014** , 2 , 2013-2019.
- [4] M. Wang, L. Xu, M. Lin, Z. Li, J. Sun, *Polym. Chem.* **2021** , 12 , 2825-2831.
- [5] X. Liu, Y. Zhang, H. Hao, W. Zhang, L. Bai, Y. Wu, H. Zhao, H. Zhang, X. Ba, *RSC Adv.* **2018** , 8 , 5776-5783.
- [6] T. Förster, *Angew. Chem. Int. Ed.* **1969** , 8 , 333-343.
- [7] M. Huang, R. Yu, K. Xu, S. Ye, S. Kuang, X. Zhu, Y. Wan, *Chem. Sci.* **2016** , 7 , 4485-4491.
- [8] J. Luo, Z. Xie, J. W. Lam, L. Cheng, H. Chen, C. Qiu, H. S. Kwok, X. Zhan, Y. Liu, D. Zhu, B. Z. Tang, *Chem. Commun. (Camb)*. **2001** , 1740-1741.
- [9] Z. Zhao, J. W. Y. Lam, B. Z. Tang, *J. Mater. Chem.* **2012** , 22 , 23726-23740.
- [10] D. Ding, K. Li, B. Liu, B. Z. Tang, *Acc. Chem. Res.* **2013** , 46 , 2441–2453.
- [11] R. T. Kwok, C. W. Leung, J. W. Lam, B. Z. Tang, *Chem. Soc. Rev.* **2015** , 44 , 4228-4238.
- [12] M. Gao, B. Z. Tang, *ACS Sens.* **2017** , 2 , 1382-1399.
- [13] S. Ge, E. Wang, J. Li, B. Z. Tang, *Macromol. Rapid. Commun.* **2022** , 43 , e2200080.
- [14] N. L. Leung, N. Xie, W. Yuan, Y. Liu, Q. Wu, Q. Peng, Q. Miao, J. W. Lam, B. Z. Tang, *Chem. Eur. J.* **2014** , 20 , 15349-15353.
- [15] G. F. Zhang, Z. Q. Chen, M. P. Aldred, Z. Hu, T. Chen, Z. Huang, X. Meng, M. Q. Zhu, *Chem. Commun. (Camb)*. **2014** , 50 , 12058-12060.
- [16] F. Zhang, H. Xie, B. Guo, C. Zhu, J. Xu, *Polym. Chem.* **2022** , 13 , 8-43.
- [17] Y. Hong, J. W. Lam, B. Z. Tang, *Chem. Soc. Rev.* **2011** , 40 , 5361-5388.

- [18] R. Hu, N. L. Leung, B. Z. Tang, *Chem. Soc. Rev.* **2014** , *43* , 4494-4562.
- [19] T. Han, D. Yan, Q. Wu, N. Song, H. Zhang, D. Wang, *Chin. J. Chem.* **2021** , *39* , 677-689.
- [20] J. Chen, Z. Xie, J. W. Y. Lam, C. C. W. Law, B. Z. Tang, *Macromolecules*. **2003** , *36* , 1108–1117.
- [21] Y. Shi, X. Cao, H. Gao, *Nanoscale*. **2016** , *8* , 4864-4881.
- [22] J. Gu, Z. Xu, D. Ma, A. Qin, B. Z. Tang, *Mater. Chem. Front.* **2020** , *4* , 1206-1211.
- [23] R. Jiang, H. Liu, M. Liu, J. Tian, Q. Huang, H. Huang, Y. Wen, Q.-y. Cao, X. Zhang, Y. Wei, *Mater. Sci. Eng. C* **2017** , *81* , 416-421.
- [24] A. Qin, J. W. Y. Lam, B. Z. Tang, *Prog. Polym. Sci.* **2012** , *37* , 182-209.
- [25] R. Zhan, Y. Pan, P. N. Manghnani, B. Liu, *Macromol. Biosci.* **2017** , *17* , 1600433.
- [26] S. Cao, J. Shao, L. K. E. A. Abdelmohsen, J. C. M. Hest, *Aggregate*. **2021** , *3* , e128.
- [27] X. Cai, B. Liu, *Angew. Chem. Int. Ed. Engl.* **2020** , *59* , 9868-9886.
- [28] M. Hu, H.-T. Feng, Y.-X. Yuan, Y.-S. Zheng, B. Z. Tang, *Coord. Chem. Rev.* **2020** , *416* , 213329.
- [29] J. Li, J. Wang, H. Li, N. Song, D. Wang, B. Z. Tang, *Chem. Soc. Rev.* **2020** , *49* , 1144-1172.
- [30] R. Hu, A. Qin, B. Z. Tang, *Prog. Polym. Sci.* **2020** , *100* , 101176.
- [31] A. Qin, J. W. Lam, B. Z. Tang, *Chem. Soc. Rev.* **2010** , *39* , 2522-2544.
- [32] Z. Qiu, T. Han, J. W. Y. Lam, B. Z. Tang, *Top. Curr. Chem. (Cham)*. **2017** , *375* , 70.
- [33] A. D. Jenkins, R. G. Jones, G. Moad, *Pure Appl. Chem.* **2009** , *82* , 483-491.
- [34] T. R. Darling, T. P. Davis, M. Fryd, A. A. Gridnev, D. M. Haddleton, S. D. Ittel, R. R. Matheson, G. Moad, E. Rizzardo, *J. Polym. Sci. A. Polym. Chem.* **2000** , *38* , 1706-1708.
- [35] D. H. Solomon, E. Rizzardo, P. Cacioli, US4581429A, **1986** .
- [36] J. Nicolas, Y. Guillaneuf, C. Lefay, D. Bertin, D. Gignes, B. Charleux, *Prog. Polym. Sci.* **2013** , *38* , 63-235.
- [37] H. Ma, L. Wang, Y. Liang, Z. Cui, P. Fu, M. Liu, X. Qiao, X. Pang, *Polym. Chem.* **2021** , *12* , 526-533.
- [38] M. Kato, M. Kamigaito, M. Sawamoto, T. Higashimura, *Macromolecules*. **1995** , *28* , 1721–1723.
- [39] J.-S. Wang, K. Matyjaszewski, *J. Am. Chem. Soc.* **1995** , *117* , 5614-5615.
- [40] V. Percec, B. Barboiu, *Macromolecules*. **1995** , *28* , 7970–7972.
- [41] K. Matyjaszewski, J.-S. Wang, US5763548A, **1998** .
- [42] K. Matyjaszewski, *Macromolecules*. **2012** , *45* , 4015-4039.
- [43] K. Matyjaszewski, L. Bombalski, W. Jakubowski, K. Min, N. V. Tsarevsky, J. Spanswick, US8404788B2, **2013** .
- [44] Z. Wang, T. Y. Yong, J. Wan, Z. H. Li, H. Zhao, Y. Zhao, L. Gan, X. L. Yang, H. B. Xu, C. Zhang, *ACS Appl. Mater. Interfaces*. **2015** , *7* , 3420-3425.
- [45] X. Guan, D. Zhang, T. Jia, Y. Zhang, L. Meng, Q. Jin, H. Ma, D. Lu, S. Lai, Z. Lei, *RSC Adv.* **2016** , *6* , 107622-107627.
- [46] T. P. Le, G. Moad, E. Rizzardo, S. H. Thang, WO1998001478A1, **1998** .
- [47] J. Chiefari, Y. K. B. Chong, F. Ercole, J. Krstina, J. Jeffery, T. P. T. Le, R. T. A. Mayadunne, G. F. Meijs, C. L. Moad, G. Moad, E. Rizzardo, S. H. Thang, *Macromolecules*. **1998** , *31* , 5559–5562.

- [48] R. Jiang, M. Liu, Q. Huang, H. Huang, Q. Wan, Y. Wen, J. Tian, Q.-y. Cao, X. Zhang, Y. Wei, *Polym. Chem.* **2017** , *8* , 7390-7399.
- [49] S. Liu, Y. Cheng, H. Zhang, Z. Qiu, R. T. K. Kwok, J. W. Y. Lam, B. Z. Tang, *Angew. Chem. Int. Ed. Engl.* **2018** , *57* , 6274-6278.
- [50] M. Tatemoto, T. Suzuki, M. Tomoda, Y. Furukawa, Y. Ueta, US4243770A, **1978** .
- [51] C. Boyer, P. Lacroix-Desmazes, J.-J. Robin, B. Boutevin, *Macromolecules.* **2006** , *39* , 4044-4053.
- [52] A. Goto, A. Ohtsuki, H. Ohfuji, M. Tanishima, H. Kaji, *J. Am. Chem. Soc.* **2013** , *135* , 11131-11139.
- [53] A. Ohtsuki, L. Lei, M. Tanishima, A. Goto, H. Kaji, *J. Am. Chem. Soc.* **2015** , *137* , 5610-5617.
- [54] S. Yamago, *Chem. Rev.* **2009** , *109* , 5051-5068.
- [55] J. P. A. Heuts, D. J. Forster, T. P. Davis, B. Yamada, H. Yamazoe, M. Azukizawa, *Macromolecules.* **1999** , *32* , 2511-2519.
- [56] A. Gridnev, *J. Polym. Sci. A. Polym. Chem.* **2000** , *38* , 1753-1766.
- [57] T. Otsu, *J. Polym. Sci. A. Polym. Chem.* **2000** , *38* , 2121-2136.
- [58] A. Bossi, M. J. Whitcombe, Y. Uludag, S. Fowler, I. Chianella, S. Subrahmanyam, I. Sanchez, S. A. Piletsky, *Biosens. Bioelectron.* **2010** , *25* , 2149-2155.
- [59] Q. Li, Y. Zhang, Z. Chen, X. Pan, Z. Zhang, J. Zhu, X. Zhu, *Org. Chem. Front.* **2020** , *7* , 2815-2841.
- [60] S. Yamago, *Proc. Jpn. Acad. Ser. B.* **2005** , *81* , 117-128.
- [61] A. Bagheri, S. Boniface, C. M. Fellows, *Chemistry Teacher International* **2021** , *3* , 19-32.
- [62] N. Corrigan, K. Jung, G. Moad, C. J. Hawker, K. Matyjaszewski, C. Boyer, *Prog. Polym. Sci.* **2020** , *111* , 101311.
- [63] S. S. Konda, J. N. Brantley, C. W. Bielawski, D. E. Makarov, *J. Chem. Phys.* **2011** , *135* , 164103.
- [64] M. F. Maitz, *Biosurf. Biotribol.* **2015** , *1* , 161-176.
- [65] M. Nitschke, S. Gramm, T. Gotze, M. Valtink, J. Drichel, B. Voit, K. Engelmann, C. Werner, *J. Biomed. Mater. Res. A.* **2007** , *80* , 1003-1010.
- [66] S. Dai, P. Ravi, K. C. Tam, *Soft Matter.* **2008** , *4* , 435-449.
- [67] Y. Zhao, *J. Mater. Chem.* **2009** , *19* , 4887-4895.
- [68] J. Wan, B. Fan, Y. Liu, T. Hsia, K. Qin, T. Junkers, B. M. Teo, S. H. Thang, *Polym. Chem.* **2020** , *11* , 3564-3572.
- [69] B. Fan, Y. Liu, J. Wan, S. Crawford, S. H. Thang, *ACS Mater. Lett.* **2020** , *2* , 492-498.
- [70] B. Fan, J. Wan, J. Zhai, X. Chen, S. H. Thang, *ACS Nano.* **2021** , *15* , 4688-4698.
- [71] J. Wan, B. Fan, S. H. Thang, *Nanoscale Adv.* **2021** , *3* , 3306-3315.
- [72] J. Wan, B. Fan, K. Putera, J. Kim, M. M. Banaszak Holl, S. H. Thang, *ACS Nano.* **2021** , *15* , 13721-13731.
- [73] K. Xu, B. Fan, K. Putera, M. Wawryk, J. Wan, B. Peng, M. M. Banaszak Holl, A. F. Patti, S. H. Thang, *Macromolecules.* **2022** , *55* , 5301-5313.
- [74] Y. Chen, Z. Sun, H. Li, Y. Dai, Z. Hu, H. Huang, Y. Shi, Y. Li, Y. Chen, *ACS Macro. Lett.* **2019** , *8* , 749-753.
- [75] X. Pang, L. Zhao, W. Han, X. Xin, Z. Lin, *Nat. Nanotechnol.* **2013** , *8* , 426-431.

- [76] Y. Liu, Z. Wang, S. Liang, Z. Li, M. Zhang, H. Li, Z. Lin, *Nano. Lett.* **2019** , *19* , 9019-9028.
- [77] B. Y. K. Chong, T. P. T. Le, G. Moad, E. Rizzardo, S. H. Thang, *Macromolecules.* **1999** , *32* , 2071-2074.
- [78] G. Moad, E. Rizzardo, S. H. Thang, *Aust. J. Chem.* **2005** , *58* , 379-410.
- [79] P. Corpart, D. Charmot, S. Z. Zard, T. Biadatti, D. Michelet, US6153705A, **2000** .
- [80] S. Z. Zard, *Macromolecules.* **2020** , *53* , 8144-8159.
- [81] C. Boyer, V. Bulmus, T. P. Davis, V. Ladmiral, J. Liu, S. Perrier, *Chem. Rev.* **2009** , *109* , 5402-5436.
- [82] M. Semsarilar, S. Perrier, *Nat. Chem.* **2010** , *2* , 811-820.
- [83] G. Moad, E. Rizzardo, S. H. Thang, *Chem. Asian. J.* **2013** , *8* , 1634-1644.
- [84] X. He, B. Wang, X. Li, J. Dong, *RSC Adv.* **2019** , *9* , 28102-28111.
- [85] D. Zhang, Y. Fan, H. Chen, S. Trepout, M. H. Li, *Angew. Chem. Int. Ed. Engl.* **2019** , *58* , 10260-10265.
- [86] X. Zhang, M. Liu, B. Yang, X. Zhang, Z. Chi, S. Liu, J. Xu, Y. Wei, *Polym. Chem.* **2013** , *4* , 5060-5064.
- [87] X. Zhang, X. Zhang, B. Yang, J. Hui, M. Liu, Z. Chi, S. Liu, J. Xu, Y. Wei, *Polym. Chem.* **2014** , *5* , 683-688.
- [88] H. Li, X. Zhang, X. Zhang, B. Yang, Y. Yang, Z. Huang, Y. Wei, *RSC Adv.* **2014** , *4* , 21588-21592.
- [89] R. Jiang, M. Liu, H. Huang, L. Mao, Q. Huang, Y. Wen, Q. Y. Cao, J. Tian, X. Zhang, Y. Wei, *J. Colloid. Interface. Sci.* **2018** , *519* , 137-144.
- [90] R. Jiang, M. Liu, T. Chen, H. Huang, Q. Huang, J. Tian, Y. Wen, Q.-y. Cao, X. Zhang, Y. Wei, *Dyes Pigm.* **2018** , *148* , 52-60.
- [91] J. Dong, M. Liu, R. Jiang, H. Huang, Q. Wan, Y. Wen, J. Tian, Y. Dai, X. Zhang, Y. Wei, *J. Colloid. Interface. Sci.* **2018** , *528* , 192-199.
- [92] Y. Liu, L. Mao, S. Yang, M. Liu, H. Huang, Y. Wen, F. Deng, Y. Li, X. Zhang, Y. Wei, *Mater. Sci. Eng. C. Mater. Biol. Appl.* **2019** , *94* , 310-317.
- [93] M. Furukawa, K. Nakabayashi, H. Mori, *J. Polym. Sci.* **2021** , *59* , 532-546.
- [94] M.-T. Weng, A. F. N. Elsyed, P.-C. Yang, M. G. Mohamed, S.-W. Kuo, K.-S. Lin, *J. Taiwan. Inst. Chem. Eng.* **2022** , *133* , 104238.
- [95] M. Liu, X. Zhang, B. Yang, F. Deng, Z. Huang, Y. Yang, Z. Li, X. Zhang, Y. Wei, *RSC Adv.* **2014** , *4* , 35137-35143.
- [96] X. Zhang, X. Zhang, B. Yang, M. Liu, W. Liu, Y. Chen, Y. Wei, *Polym. Chem.* **2014** , *5* , 356-360.
- [97] Z. Huang, X. Zhang, X. Zhang, B. Yang, Y. Zhang, K. Wang, J. Yuan, L. Tao, Y. Wei, *Polym. Chem.* **2015** , *6* , 2133-2138.
- [98] Z. Huang, X. Zhang, X. Zhang, S. Wang, B. Yang, K. Wang, J. Yuan, L. Tao, Y. Wei, *RSC Adv.* **2015** , *5* , 89472-89477.
- [99] Y. Chen, H. Han, H. Tong, T. Chen, H. Wang, J. Ji, Q. Jin, *ACS Appl. Mater. Interfaces.* **2016** , *8* , 21185-21192.
- [100] Q. Y. Cao, R. Jiang, M. Liu, Q. Wan, D. Xu, J. Tian, H. Huang, Y. Wen, X. Zhang, Y. Wei, *Mater. Sci. Eng. C. Mater. Biol. Appl.* **2017** , *80* , 578-583.
- [101] Y. Liu, L. Mao, X. Liu, M. Liu, D. Xu, R. Jiang, F. Deng, Y. Li, X. Zhang, Y. Wei, *Mater. Sci. Eng. C. Mater. Biol. Appl.* **2017** , *79* , 590-595.

- [102] Y. Liu, L. Mao, S. Yang, M. Liu, H. Huang, Y. Wen, F. Deng, Y. Li, X. Zhang, Y. Wei, *Dyes Pigm.* **2018** , *158* , 79-87.
- [103] Y. Chen, Z. Huang, X. Liu, L. Mao, J. Yuan, X. Zhang, L. Tao, Y. Wei, *RSC Adv.* **2019** , *9* , 32601-32607.
- [104] H. Li, X. Zhang, X. Zhang, B. Yang, Y. Yang, Y. Wei, *Polym. Chem.* **2014** , *5* , 3758-3762.
- [105] G. Zeng, M. Liu, R. Jiang, Q. Huang, L. Huang, Q. Wan, Y. Dai, Y. Wen, X. Zhang, Y. Wei, *Mater. Sci. Eng. C. Mater. Biol. Appl.* **2018** , *83* , 154-159.
- [106] B. Shi, J. Lü, Y. Liu, Y. Xiao, C. Lü, *Polym. Chem.* **2021** , *12* , 3775-3783.
- [107] W. Shi, B. Wu, X. Guo, A. Feng, S. H. Thang, *Polym. Chem.* **2022** , *13* , 2026-2035.
- [108] C. Ma, Q. Ling, S. Xu, H. Zhu, G. Zhang, X. Zhou, Z. Chi, S. Liu, Y. Zhang, J. Xu, *Macromol. Biosci.* **2014** , *14* , 235-243.
- [109] L. Huang, M. Liu, L. Mao, X. Zhang, D. Xu, Q. Wan, Q. Huang, Y. Shi, F. Deng, X. Zhang, Y. Wei, *Mater. Sci. Eng. C. Mater. Biol. Appl.* **2017** , *76* , 586-592.
- [110] Z. Long, L. Mao, M. Liu, Q. Wan, Y. Wan, X. Zhang, Y. Wei, *Polym. Chem.* **2017** , *8* , 5644-5654.
- [111] Z. Huang, X. Zhang, X. Zhang, S. Wang, B. Yang, K. Wang, J. Yuan, L. Tao, Y. Wei, *Polym. Bull.* **2017** , *74* , 4525-4536.
- [112] Y. Zhao, Y. Wu, S. Chen, H. Deng, X. Zhu, *Macromolecules.* **2018** , *51* , 5234-5244.
- [113] Q. Li, X. Li, Z. Wu, Y. Sun, J. Fang, D. Chen, *Polym. Chem.* **2018** , *9* , 4150-4160.
- [114] Z. Huang, Y. Chen, R. Wang, C. Zhou, X. Liu, L. Mao, J. Yuan, L. Tao, Y. Wei, *RSC Adv.* **2020** , *10* , 5704-5711.
- [115] Y.-G. Jia, K.-F. Chen, M. Gao, S. Liu, J. Wang, X. Chen, L. Wang, Y. Chen, W. Song, H. Zhang, L. Ren, X.-X. Zhu, B. Z. Tang, *Sci. China Chem.* **2020** , *64* , 403-407.
- [116] S. Zhou, P. Gu, H. Wan, Y. Zhu, A. Wang, H. Shi, Q. Xu, J. Lu, *Polym. Chem.* **2020** , *11* , 7244-7252.
- [117] Z. Huang, Y. Chen, C. Zhou, K. Wang, X. Liu, L. Mao, J. Yuan, L. Tao, Y. Wei, *Dyes Pigm.* **2021** , *184* , 108829.
- [118] Z. Huang, C. Zhou, W. Chen, J. Li, M. Li, X. Liu, L. Mao, J. Yuan, L. Tao, Y. Wei, *Dyes Pigm.* **2021** , *196* , 109793.
- [119] C. Ma, G. Xie, Y. Tao, H. Zhu, Y. Zhang, Z. Chi, S. Liu, J. Xu, *Dyes Pigm.* **2021** , *184* , 108776.
- [120] Z. Huang, R. Wang, Y. Chen, X. Liu, K. Wang, L. Mao, K. Wang, J. Yuan, X. Zhang, L. Tao, Y. Wei, *Polym. Chem.* **2019** , *10* , 2162-2169.
- [121] Q. Wan, R. Jiang, L. Mao, D. Xu, G. Zeng, Y. Shi, F. Deng, M. Liu, X. Zhang, Y. Wei, *Mater. Chem. Front.* **2017** , *1* , 1051-1058.
- [122] M. Huo, Q. Ye, H. Che, X. Wang, Y. Wei, J. Yuan, *Macromolecules.* **2017** , *50* , 1126-1133.
- [123] B. Fan, J. Wan, J. Zhai, N. K. S. Teo, A. Huynh, S. H. Thang, *Polym. Chem.* **2022** , *13* , 4333-4342.
- [124] L. Qiu, H. Zhang, B. Wang, Y. Zhan, C. Xing, C. Y. Pan, *ACS Appl. Mater. Interfaces.* **2020** , *12* , 1348-1358.
- [125] S. Han, Y. Gu, M. Ma, M. Chen, *Chem. Sci.* **2020** , *11* , 10431-10436.
- [126] Y. Zhou, Z. Wang, Y. Wang, L. Li, N. Zhou, Y. Cai, Z. Zhang, X. Zhu, *Polym. Chem.* **2020** , *11* , 5619-5629.

- [127] A. Zhang, J. Hao, S. Hou, G. Shi, Y. He, Z. Cui, M. Liu, X. Qiao, P. Fu, X. Pang, *J. Polym. Res.* **2022** , *29* , 127.
- [128] Z. Huo, L. Zhuang, G. Shi, Y. He, Z. Cui, P. Fu, M. Liu, X. Qiao, X. Pang, *J. Colloid. Interface. Sci.* **2021** , *600* , 421-429.
- [129] J. Chen, M. Liu, Q. Huang, L. Huang, H. Huang, F. Deng, Y. Wen, J. Tian, X. Zhang, Y. Wei, *J. Chem. Eng.* **2018** , *337* , 82-90.
- [130] S. Li, C. Gao, *Polym. Chem.* **2013** , *4* , 4450-4460.
- [131] T. G. Ribelli, F. Lorandi, M. Fantin, K. Matyjaszewski, *Macromol. Rapid. Commun.* **2019** , *40* , e1800616.
- [132] M. S. Kharasch, W. H. Urry, E. V. Jensen, *J. Am. Chem. Soc.* **1945** , *67* , 1626.
- [133] R. M. Pearson, C. H. Lim, B. G. McCarthy, C. B. Musgrave, G. M. Miyake, *J. Am. Chem. Soc.* **2016** , *138* , 11399-11407.
- [134] C. H. Lim, M. D. Ryan, B. G. McCarthy, J. C. Theriot, S. M. Sartor, N. H. Damrauer, C. B. Musgrave, G. M. Miyake, *J. Am. Chem. Soc.* **2017** , *139* , 348-355.
- [135] J. Kreutzer, Y. Yagci, *Polymers (Basel)*. **2017** , *10* , 35.
- [136] H. Deng, R. Hu, E. Zhao, C. Y. K. Chan, J. W. Y. Lam, B. Z. Tang, *Macromolecules.* **2014** , *47* , 4920-4929.
- [137] X. Guan, L. Meng, Q. Jin, B. Lu, Y. Chen, Z. Li, L. Wang, S. Lai, Z. Lei, *Macromol. Mater. Eng.* **2018** , *303* , 1700553.
- [138] C.-T. Lai, R.-H. Chien, S.-W. Kuo, J.-L. Hong, *Macromolecules.* **2011** , *44* , 6546-6556.
- [139] Y.-H. Zhang, P.-Y. Gu, J.-B. Zhou, Y.-J. Xu, W. Liu, Q.-F. Gu, D.-Y. Chen, N.-J. Li, Q.-F. Xu, J.-M. Lu, *J. Mater. Chem. C*. **2014** , *2* , 2082-2088.
- [140] Z. Zhang, P. Bilalis, H. Zhang, Y. Gnanou, N. Hadjichristidis, *Macromolecules.* **2017** , *50* , 4217-4226.
- [141] Z. Zhang, N. Hadjichristidis, *ACS Macro. Lett.* **2018** , *7* , 886-891.
- [142] H. Wan, P. Gu, F. Zhou, H. Wang, J. Jiang, D. Chen, Q. Xu, J. Lu, *Polym. Chem.* **2018** , *9* , 3893-3899.
- [143] M. Feng, L. Fang, F. Guan, S. Huang, Y. Cheng, Y. Liang, H. Zhang, *Polymers (Basel)*. **2018** , *10* , 722.
- [144] W. Feng, G. Li, L. Tao, Y. Wei, X. Wang, *Colloids. Surf. B. Biointerfaces.* **2021** , *202* , 111687.
- [145] Y. Jiang, N. Hadjichristidis, *Macromolecules.* **2019** , *52* , 1955-1964.
- [146] Y. Jiang, N. Hadjichristidis, *Chinese. J. Polym. Sci.* **2019** , *37* , 930-935.
- [147] W. Liu, Q. Yang, Y. Yang, F. Xing, P. Xiao, *Ind. Eng. Chem. Res.* **2021** , *60* , 7024-7032.
- [148] D.-J. Yang, L.-Y. Lin, P.-C. Huang, J.-Y. Gao, J.-L. Hong, *React. Funct. Polym.* **2016** , *108* , 47-53.
- [149] W. Zhuang, B. Ma, G. Liu, G. Li, Y. Wang, *J. Appl. Polym. Sci.* **2018** , *135* , 45651.
- [150] J. Dong, R. Jiang, W. Wan, H. Ma, H. Huang, Y. Feng, Y. Dai, H. Ouyang, X. Zhang, Y. Wei, *Appl. Surf. Sci.* **2020** , *508* , 144799.
- [151] P. Y. Gu, C. J. Lu, F. L. Ye, J. F. Ge, Q. F. Xu, Z. J. Hu, N. J. Li, J. M. Lu, *Chem. Commun. (Camb)*. **2012** , *48* , 10234-10236.
- [152] W. Yuan, P.-Y. Gu, C.-J. Lu, K.-Q. Zhang, Q.-F. Xu, J.-M. Lu, *RSC Adv.* **2014** , *4* , 17255-17261.

- [153] R. Mori, G. Iasilli, M. Lessi, A. B. Muñoz-García, M. Pavone, F. Bellina, A. Pucci, *Polym. Chem.* **2018** , *9* , 1168-1177.
- [154] X. Wang, X. Qiao, X. Yin, Z. Cui, P. Fu, M. Liu, G. Wang, X. Pan, X. Pang, *Chem. Asian. J.* **2020** , *15* , 1014-1017.
- [155] Y. Tang, Z. Zhao, A. Qin, D. Wang, B. Z. Tang, *Matter.***2021** , *4* , 2587-2589.
- [156] C. Ma, T. Han, N. Niu, L. Al-Shok, S. Efstathiou, D. Lester, S. Huband, D. Haddleton, *Polym. Chem.* **2022** , *13* , 58-68.
- [157] P.-Y. Gu, C.-J. Lu, Z.-J. Hu, N.-J. Li, T.-t. Zhao, Q.-F. Xu, Q.-H. Xu, J.-D. Zhang, J.-M. Lu, *J. Mater. Chem. C.***2013** , *1* , 2599-2606.
- [158] S. Wang, B. Jin, G. Chen, Y. Luo, X. Li, *Polym. Chem.***2020** , *11* , 4706-4713.
- [159] T.-L. Nghiem, S. Riebe, I. Maisuls, C. A. Strassert, J. Voskuhl, A. H. Gröschel, *Polymer.* **2020** , *208* , 122942.
- [160] Z. Huang, X. Zhang, X. Zhang, S. Wang, B. Yang, K. Wang, J. Yuan, L. Tao, Y. Wei, *RSC Adv.* **2015** , *5* , 65884-65889.
- [161] G. Qi, F. Hu, Kenry, K. C. Chong, M. Wu, Y. H. Gan, B. Liu, *Adv. Funct. Mater.* **2020** , *30* , 2001338.
- [162] L. Fang, C. Huang, G. Shabir, J. Liang, Z. Liu, H. Zhang, *ACS Macro. Lett.* **2019** , *8* , 1605-1610.
- [163] L. Mao, X. Liu, M. Liu, L. Huang, D. Xu, R. Jiang, Q. Huang, Y. Wen, X. Zhang, Y. Wei, *Appl. Surf. Sci.* **2017** , *419* , 188-196.
- [164] L. Huang, S. Yu, W. Long, H. Huang, Y. Wen, F. Deng, M. Liu, W. Xu, X. Zhang, Y. Wei, *Microporous. Mesoporous. Mater.***2020** , *308* , 110520.
- [165] M. Kopeć, M. Pikiel, G. J. Vancso, *Polym. Chem.***2020** , *11* , 669-674.
- [166] Q. Zhou, B. Cao, C. Zhu, S. Xu, Y. Gong, W. Z. Yuan, Y. Zhang, *Small.* **2016** , *12* , 6586-6592.
- [167] W. Zhang Yuan, Y. Zhang, *J. Polym. Sci. A. Polym. Chem.***2017** , *55* , 560-574.
- [168] K. Matyjaszewski, S. Coca, S. G. Gaynor, M. Wei, B. E. Woodworth, *Macromolecules.* **1997** , *30* , 7348-7350.
- [169] V. Percec, T. Guliashvili, J. S. Ladislaw, A. Wistrand, A. Stjern Dahl, M. J. Sienkowska, M. J. Monteiro, S. Sahoo, *J. Am. Chem. Soc.* **2006** , *128* , 14156-14165.
- [170] M. K. Georges, R. P. N. Veregin, P. M. Kazmaier, G. K. Hamer, *Macromolecules.* **1993** , *26* , 2987-2988.
- [171] Y. K. Chong, F. Ercole, G. Moad, E. Rizzardo, S. H. Thang, A. G. Anderson, *Macromolecules.* **1999** , *32* , 6895-6903.
- [172] C. J. Hawker, A. W. Bosman, E. Harth, *Chem. Rev.***2001** , *101* , 3661-3688.
- [173] D. Bertin, D. Gimes, S. R. Marque, P. Tordo, *Chem. Soc. Rev.* **2011** , *40* , 2189-2198.
- [174] D. Li, J. Chen, M. Hong, Y. Wang, D. M. Haddleton, G. Z. Li, Q. Zhang, *Biomacromolecules.* **2021** , *22* , 2224-2232.
- [175] C. M. Tonge, E. R. Sauvé, N. R. Paisley, J. E. Heyes, Z. M. Hudson, *Polym. Chem.* **2018** , *9* , 3359-3367.
- [176] J. F. Wang, G. E. Jabbour, E. A. Mash, J. Anderson, Y. Zhang, P. A. Lee, N. R. Armstrong, N. Peyghambarian, B. Kippelen, *Adv. Mater.* **1999** , *11* , 1266-1269.
- [177] A. Facchetti, *Mater. Today.* **2013** , *16* , 123-132.
- [178] B. Sun, W. Hong, Z. Yan, H. Aziz, Y. Li, *Adv. Mater.***2014** , *26* , 2636-2642.

- [179] S. Griggs, A. Marks, H. Bristow, I. McCulloch, *J. Mater. Chem. C* **2021** , 9 , 8099-8128.
- [180] E. R. Sauve, C. M. Tonge, Z. M. Hudson, *J. Am. Chem. Soc.* **2019** , 141 , 16422-16431.
- [181] S. Naghibi, S. Sabouri, Y. Hong, Z. Jia, Y. Tang, *Biosensors (Basel)*. **2022** , 12 , 373.
- [182] X. Gao, J. Cao, Y. Song, X. Shu, J. Liu, J. Z. Sun, B. Liu, B. Z. Tang, *RSC Adv.* **2018** , 8 , 10975-10979.
- [183] Z. Wei, D. Chen, X. Zhang, L. Wang, W. Yang, *Macromolecules*. **2022** , 55 , 2911-2923.
- [184] J. Poisson, C. M. Tonge, N. R. Paisley, E. R. Sauv e, H. McMillan, S. V. Halldorson, Z. M. Hudson, *Macromolecules*. **2021** , 54 , 2466-2476.
- [185] C. M. Tonge, N. R. Paisley, A. M. Polgar, K. Lix, W. R. Algar, Z. M. Hudson, *ACS Appl. Mater. Interfaces*. **2020** , 12 , 6525-6535.
- [186] C. J. Christopherson, D. M. Mayder, J. Poisson, N. R. Paisley, C. M. Tonge, Z. M. Hudson, *ACS Appl. Mater. Interfaces*. **2020** , 12 , 20000-20011.
- [187] Y. Bao, H. De Keersmaecker, S. Corneillie, F. Yu, H. Mizuno, G. Zhang, J. Hofkens, B. Mendrek, A. Kowalczyk, M. Smet, *Chem. Mater.* **2015** , 27 , 3450-3455.
- [188] Y. Bao, E. Guegain, V. Nicolas, J. Nicolas, *Chem. Commun. (Camb)*. **2017** , 53 , 4489-4492.
- [189] S. Banerjee, E. B. Veale, C. M. Phelan, S. A. Murphy, G. M. Tocci, L. J. Gillespie, D. O. Frimannsson, J. M. Kelly, T. Gunnlaugsson, *Chem. Soc. Rev.* **2013** , 42 , 1601-1618.
- [190] W. Qin, D. Ding, J. Liu, W. Z. Yuan, Y. Hu, B. Liu, B. Z. Tang, *Adv. Funct. Mater.* **2012** , 22 , 771-779.
- [191] J. Mei, N. L. Leung, R. T. Kwok, J. W. Lam, B. Z. Tang, *Chem. Rev.* **2015** , 115 , 11718-11940.
- [192] K. Li, Y. Lin, C. Lu, *Chem. Asian. J.* **2019** , 14 , 715-729.
- [193] L. Wang, L. Wang, J. Wu, L. Wang, W. Cong, X. Wang, R. Hu, W. Li, M. Tebyetekerwa, B. Z. Tang, *Prog. Org. Coat.* **2021** , 159 , 106448.
- [194] X. Zhang, X. Zhang, B. Yang, Y. Zhang, Y. Wei, *ACS Appl. Mater. Interfaces*. **2014** , 6 , 3600-3606.
- [195] J. Li, H. Wang, B. Yang, L. Xu, N. Zheng, H. Chen, S. Li, *Mater. Sci. Eng. C. Mater. Biol. Appl.* **2016** , 58 , 273-277.
- [196] Y. Bae, S. Fukushima, A. Harada, K. Kataoka, *Angew. Chem.* **2003** , 115 , 4788-4791.
- [197] X. Li, X. Gao, W. Shi, H. Ma, *Chem. Rev.* **2014** , 114 , 590-659.
- [198] Y. B. Hu, J. W. Y. Lam, B. Z. Tang, *Chinese. J. Polym. Sci.* **2019** , 37 , 289-301.

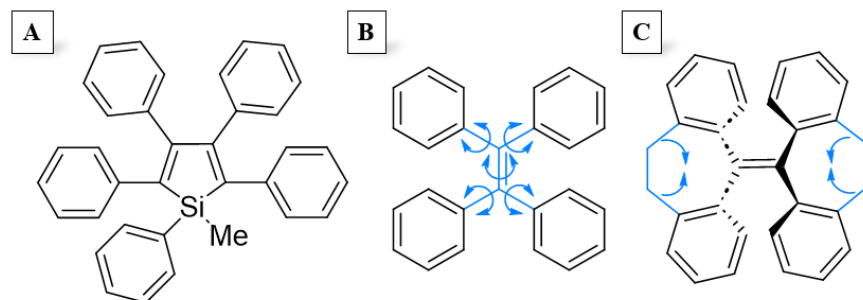


Figure 1. (A) Chemical structure of 1-methy-1,2,3,4,5-pentaphenylsilole. Adapted with permission.^[8] Copyright 2001, Royal Society of Chemistry (B) Restriction of Intramolecular Rotation (RIR) effect of 1,1,2,2-tetraphenylethene (TPE), and (C) Restriction of Intramolecular Vibration (RIV) effect of 10,10',11,11'-tetrahydro-5,5'-bidibenzo[*a,d*][7]annulenyldiene (THBDBA). Adapted with permission.^[13] Copyright 2022, Wiley-VCH.

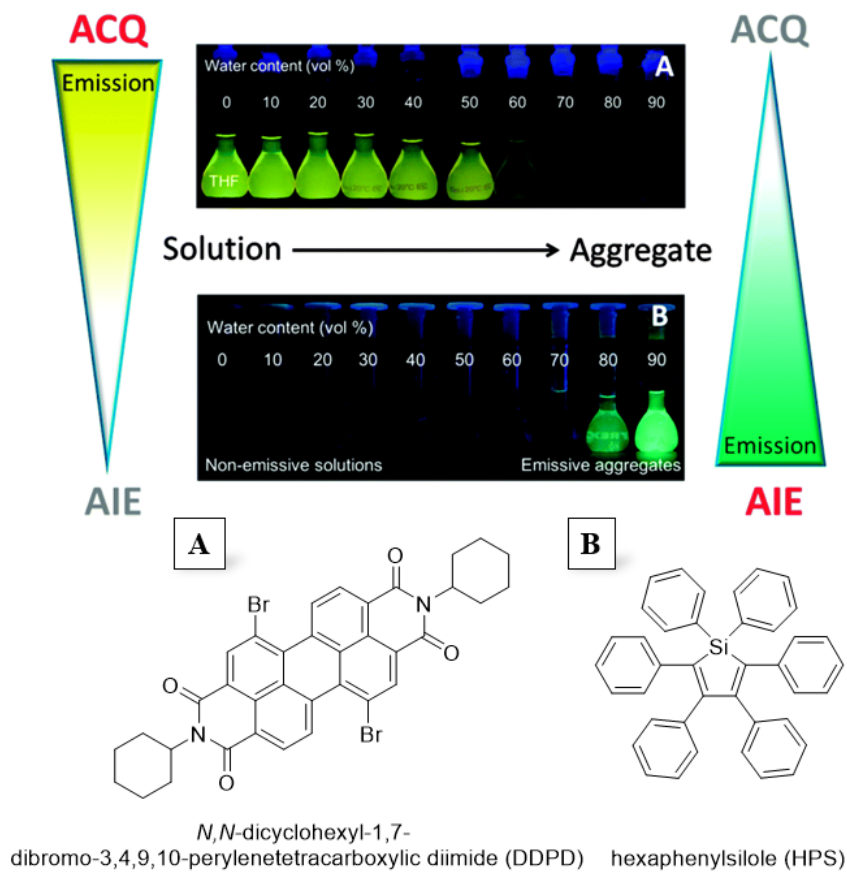


Figure 2. Fluorescence photographs of solutions/suspensions and chemical structure of (A) DDPD and (B) HPS in THF–water mixtures with different water contents demonstrating Aggregation-Caused Quenching (ACQ) and Aggregation-Induced Emission (AIE) respectively. Adapted with permission.^[18] Copyright 2014, Royal Society of Chemistry.

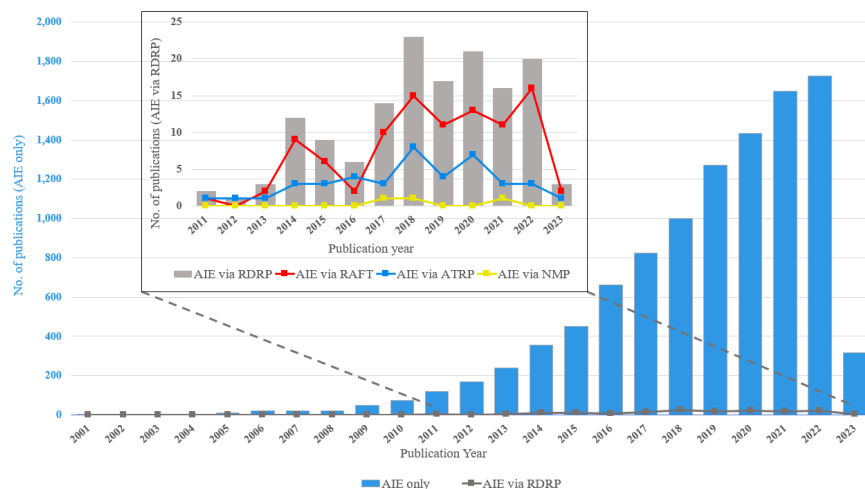
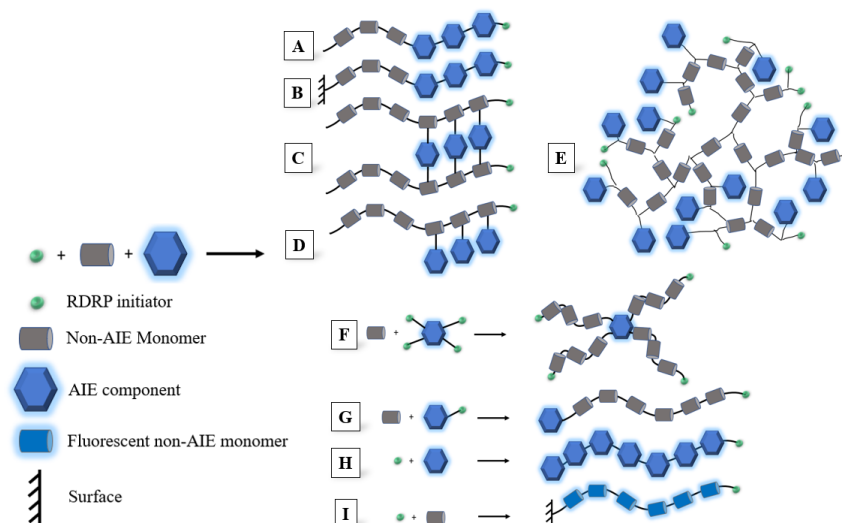


Figure 3 . Number of publications on AIE for the years 2001 – 2023. Source - SciFinder[®] 24/02/2023, re-search topic: “Aggregation Induced Emission”, AIE, command string keywords: “Aggregation-induced emission or Aggregation-induced emission enhancement or AIEgen or AIEE or AIEEgen or AIENP” with filter “publication year 2001 to 2023”, (“Controlled radical polym*” or “Reversible-deactivation radical polymerization” or RDRP or ”living” radical polymerization”) and (Aggregation-induced emission or Aggregation-induced emission enhancement or AIEgen or AIEE or AIEEgen or AIENP or AIE)”, (“Nitroxides, radicals and polym*”) or “Nitroxide-mediated polymerization” or “Nitroxide mediated polymerization” or Nitroxides, radicals and (Aggregation-induced emission or Aggregation-induced emission enhancement or AIEgen or AIEE or AIEEgen or AIENP or AIE)”, (“ATRP and polym*”) or Atom transfer radical polymerization or Living atom transfer radical polymerization and (Aggregation-induced emission or Aggregation-induced emission enhancement or AIEgen or AIEE or AIEEgen or AIENP or AIE)”, (“RAFT and polym*”) or RAFT polymerization or RAFT polymerization kinetics or RAFT polymerization catalyst or “Reversible addition fragmentation chain transfer” or RAFT and (Aggregation-induced emission or Aggregation-induced emission enhancement or AIEgen or AIEE or AIEEgen or AIENP or AIE)”.



Scheme 1 . Possible polymerization reactions via RDRP to synthesize polymers.

Table 1 . Overview of different RDRP techniques utilized with selected monomers, RAFT agents/ATRP initiators to synthesize AIE polymers.

| Entry | Reaction type | Monomer | RAFT agent/ATRP initiator | Reference |
|-----------------|----------------|---------|---------------------------|------------|
| 1 | RAFT | | | [122] |
| 2 | RAFT | | | [84] |
| 3 | RAFT | | | [123] |
| 4 | RAFT | | | [85] |
| 5 | RAFT | | | [124] |
| 6 | RAFT | | | [120] |
| 7 | RAFT | | | [128] |
| 8 | RAFT | | | [5] |
| 9 | RAFT | | | [86] |
| 10 | RAFT | | | [94] |
| 11 | RAFT | | | [121, 198] |
| 12 | ATRP | | | [45] |
| 13 | ATRP | | | [137] |
| 14 ^a | ATRP | | | [145, 146] |
| 15 | ATRP | | | [149] |
| 16 | ATRP | | | [147] |
| 17 | ATRP | | | [150] |
| 18 | ATRP | | | [148] |
| 19 ^b | ATRP | | | [151] |
| 20 | ATRP | | | [157] |
| 21 ^c | ATRP | | | [165, 167] |
| 22 | Others (Cu(0)) | | | [174] |
| 23 ^d | Others (Cu(0)) | | | [175] |
| 24 ^e | Others (Cu(0)) | | | [180] |
| 25 | Others (Cu(0)) | | | [181] |
| 26 | Others (NMP) | | | [188] |

^a Block copolymer synthesis using two different monomers separately. ^{b, d, e} Block copolymer synthesis using three different monomers separately. ^c Non-AIE-active monomer which can be polymerized via ATRP to yield AIE-active polymer with unusual AIE fluorescence behavior.

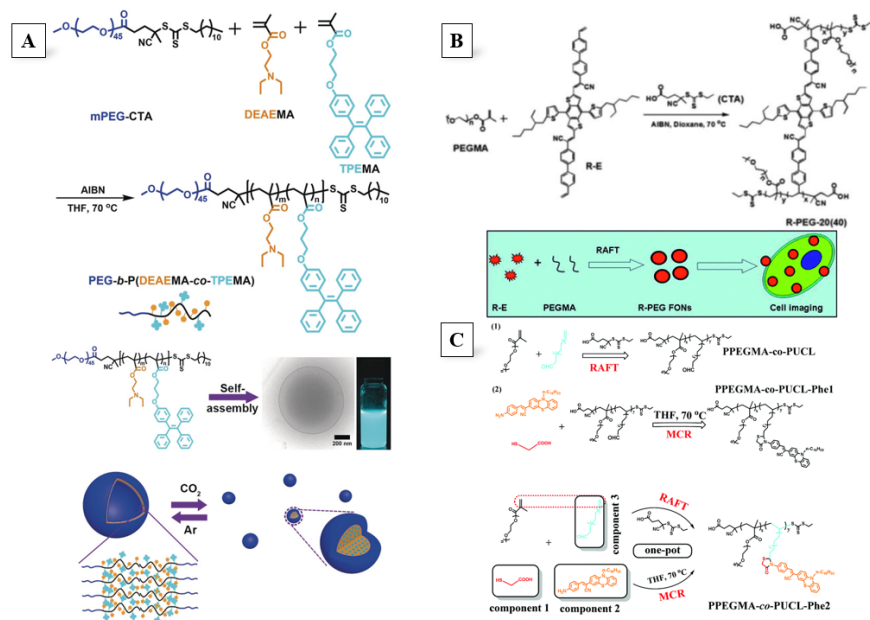


Figure 4 . (A) RAFT polymerization of CO₂-responsive amphiphilic block copolymer PEG-*b*-P(DEAEMA-*co*-TPEMA), and their self-assembly behavior into AIE fluorescent polymersomes, with cryo EM image of PEG₄₅-*b*-P(DEAEMA₃₆-*co*-TPEMA₆) polymersomes formed in dioxane/water system, with photograph taken of the final polymersomes in water irradiated by UV light ($I = 365$ nm). Molecular organization in vesicular membrane shown in the reversible polymersome–micelle transition upon CO₂/Ar treatment. Reproduced with permission: Copyright 2019, Angewandte Chemie.^[85] (B) RAFT polymerization of R-PEG-20 and R-PEG-40 completed with schematic illustration showing the cell imaging applications of R-PEG FPNs. Reproduced with permission: Copyright 2013, Royal Society of Chemistry.^[86] (C) Step-wise preparation of a fluorescent polymer (PPEGMA-*co*-PUCL-Phe1) and efficient one-pot preparation of the same fluorescent polymer (PPEGMA-*co*-PUCL-Phe2). Reproduced with permission: Copyright 2016, Royal Society of Chemistry.^[121]

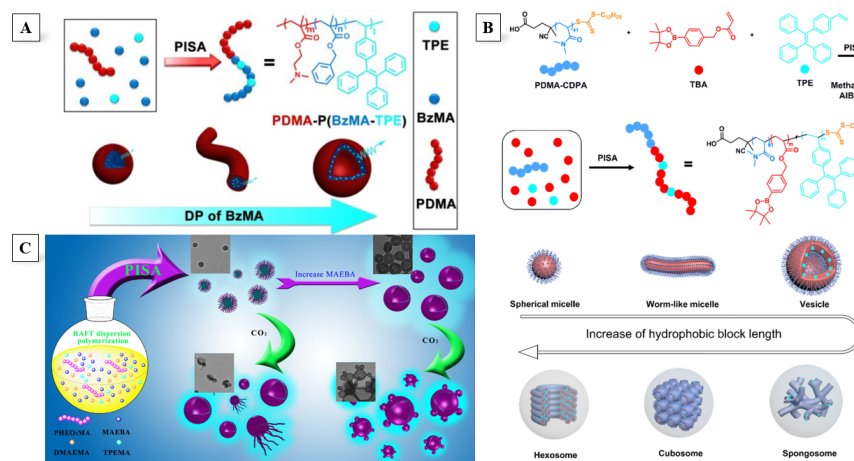


Figure 5 . (A) Preparation of AIE-active PDMA-P(BzMA-TPE) assemblies by PISA. Reproduced with permission: Copyright 2017, American Chemical Society.^[122] (B) Synthetic scheme of the block copolymer

PDMA₄₁-*b*-P(TBA-*r*-TPE)_x based fluorescent nano/micro-objects via PISA, and the structure of each type of morphologies achieved via PISA with increasing of the hydrophobic chain length. Reproduced with permission: Copyright 2022, Royal Society of Chemistry.^[123] (C) RAFT dispersion polymerization PISA of CO₂-Responsive P(HEO₂MA)₄₀-P(MAEBMA-DMAEMA-TPEMA) polymeric nano-objects, exhibiting morphology evolution and fluorescence variation induced by CO₂. Reproduced with permission: Copyright 2019, American Chemical Society.^[124]

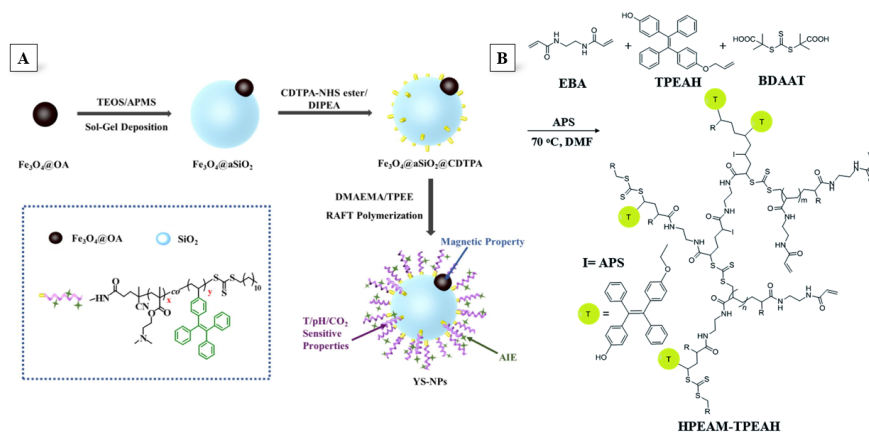


Figure 6 . (A) Fabrication of YS-NPs via sol-gel deposition and SI-RAFT polymerization. Reproduced with permission: Copyright 2021, Elsevier.^[128] (B) Synthesis of HPEAM-TPEAH from EBA, TPEAH and BDAAT. Reproduced with permission: Copyright 2018, Royal Society of Chemistry.^[5]

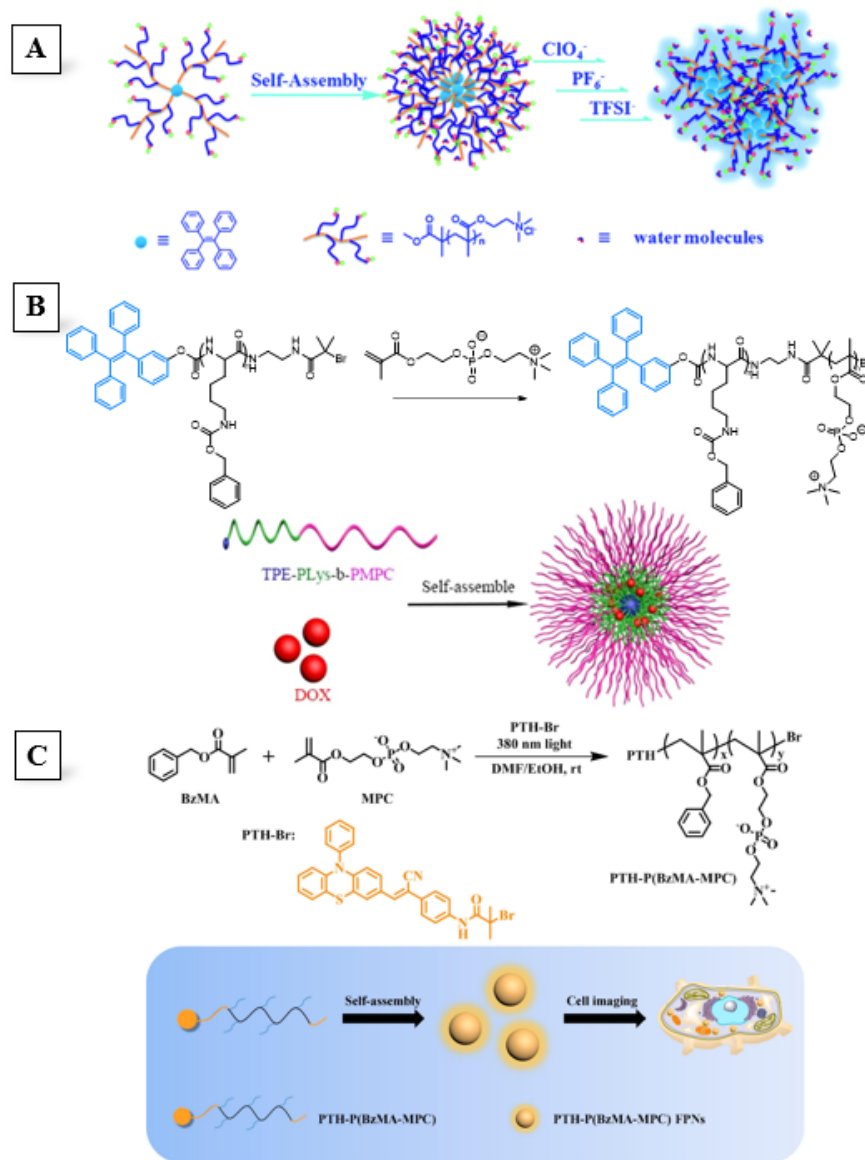


Figure 7 . (A) Illustration of the self-assembly behavior of TPE-PMETAC in pure water after adding different types of counterions. Reproduced with permission: Copyright 2016, Royal Society of Chemistry.^[45] (B) Illustration of preparation of DOX-loaded TPE-PLys-*b* -PMPC micelles. Reproduced with permission: Copyright 2017, Wiley-VCH.^[149] (C) Illustration showing the preparation of fluorescent PTH-P(BzMA-MPC) copolymers and their self-assembly behavior into FPNS in aqueous solution, where the resulting AIE-active FPNS were used for cell imaging. Reproduced with permission: Copyright 2020, Elsevier.^[150]

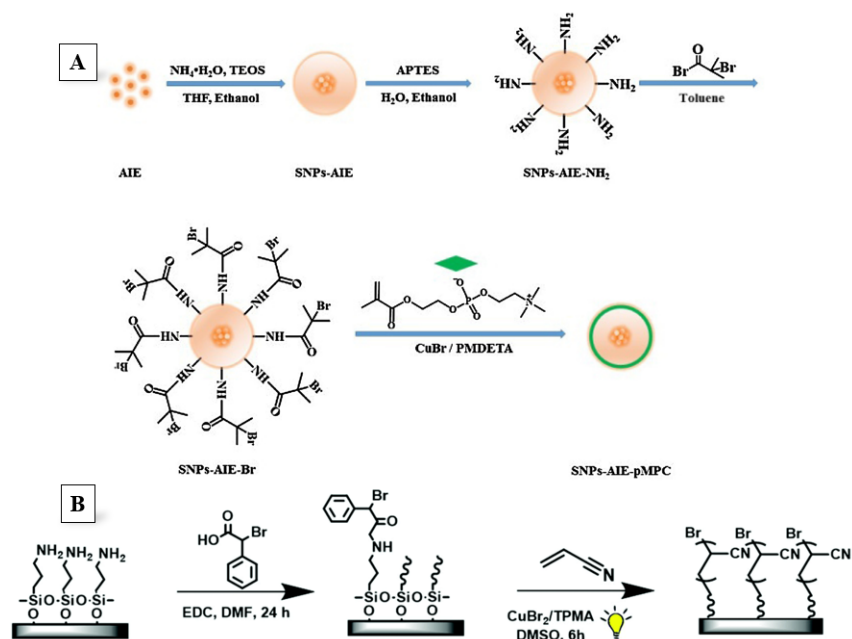


Figure 8. (A) Illustration showing the synthesis of SNPs-AIE and SNPs-AIE functionalized with pMPC. Reproduced with permission: Copyright 2017, Elsevier ^[163](B) Illustration of the synthetic route to PAN brushes by photoinduced SI-ATRP. Reproduced with permission: Copyright 2020, Royal Society of Chemistry.^[165]

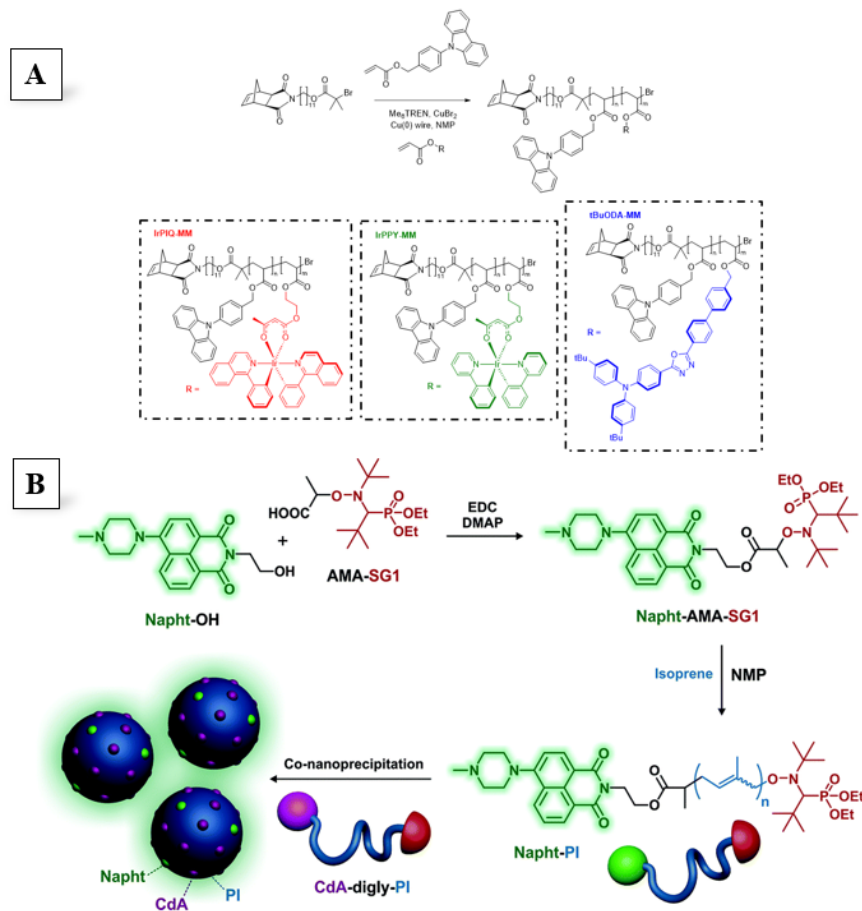


Figure 9 . (A) Cu(0)-RDRP of norbornene-functionalized red, green, and blue emissive macromonomers (NMP = *N*-methyl-2-pyrrolidone, Me₆TREN = Tris[2-(dimethylamino)ethyl]amine). Reproduced with permission: Copyright 2019, American Chemical Society.^[180] **(B)** Synthesis of 4-(*N*-methylpiperazine)-1,8-naphthalimide-polyisoprene (Napht-PI) conjugate via NMP and its co-nanoprecipitation with cladribine-diglycolate-polyisoprene (CdAdigly-PI) to form AIE-active produg nanoparticles. Reproduced with permission: Copyright 2017, Royal Society of Chemistry.^[188]

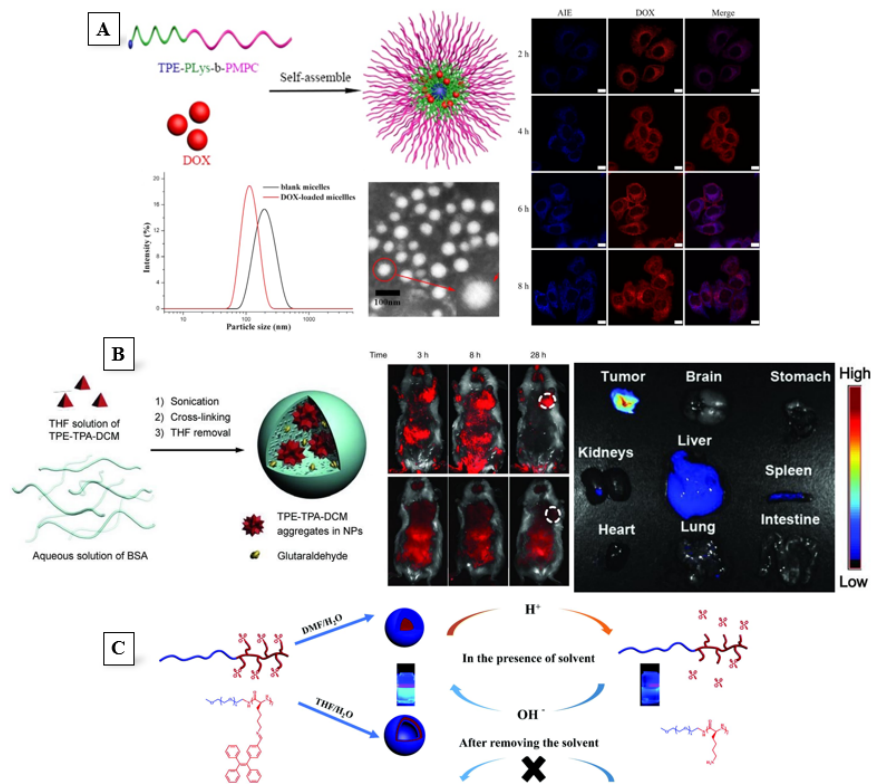


Figure 10 . (A) Illustration of self-assembly behavior of DOX-loaded TPE-PLys-*b* -PMPC micelles, along with particle size distribution determined by DLS, the typical morphology of the polymer micelles detected by TEM, and CLSM images of DOX-loaded micelles after incubation with HeLa cells for 2, 4, 6, and 8 h. The DOX concentration is 10 $\mu\text{g}/\text{mL}$ (scale bar in images was 10 μm). Reproduced with permission: Copyright 2017, Wiley-VCH.^[149] **(B)** Illustration of preparing TPE-TPA-DCM-loaded BSA NPs, along with *in vivo* non-invasive fluorescence imaging of H₂₂-tumorbearing mice after intravenous injection of TPE-TPA-DCM-loaded BSA NPs (with TPE-TPA-DCM loading of 0.86 wt%) (upper picture) and bare TPE-TPA-DCM NPs (lower picture) at same TPE-TPA-DCM concentration (white circles mark the tumor sites). *Ex vivo* fluorescence imaging on tumor tissue and major organs of mice treated with fluorogen-loaded BSA NPs, which were sacrificed at 24 h post-injection. Reproduced with permission: Copyright 2011, Wiley-VCH.^[190] **(C)** The pH-responsive AIE process assisted by the self-assembly of block copolymers. Reproduced with permission: Copyright 2021, Royal Society of Chemistry.^[4]

Author Biographies



Nicholas Kai Shiang Teo received his bachelor's degree (with honours) from Nanyang Technological University, Singapore (NTU) and is now pursuing his PhD degree in Chemistry at Monash University, Australia Melbourne. His research interests include exploring new polymer-metal nanocomposites and luminescent polymeric materials.

Hosted file

image72.emf available at <https://authorea.com/users/609837/articles/639038-aggregation-induced-emission-polymers-via-reversible-deactivation-radical-polymerization>

Dr Bo Fan is a Research Fellow at Monash University. He received his PhD in Chemical and Biochemical Engineering from the University of Western Ontario in 2018. His research interests include controlled radical polymerization, polymerization-induced self-assembly (PISA), stimuli-responsive polymers and their applications in drug delivery and mineral beneficiation.



Dr Aditya Ardana completed his PhD in Polymer Chemistry and Bioengineering from the University of Queensland in 2016. After finishing his fellowship at CSIRO (2018-2022), he joined the group of Prof San Thang at Monash University. His research interests include reversible addition-fragmentation chain-transfer (RAFT) polymerization, protein chemistry, bioconjugation and applications of polymer conjugates in drug delivery and mineral beneficiation.

Hosted file

image74.emf available at <https://authorea.com/users/609837/articles/639038-aggregation-induced-emission-polymers-via-reversible-deactivation-radical-polymerization>

Prof. San H. Thang completed his PhD in chemistry at Griffith University in 1987. After a research career at CSIRO (1986–2014), he is currently a Professor of Chemistry at Monash University. His research focuses on the interface between biology and polymer chemistry. He is responsible for several key inventions in the area of controlled/living radical polymerization; significantly, he is a co-inventor of the RAFT (Reversible Addition–Fragmentation Chain Transfer) process. In June 2018, he was awarded the Companion in the General Division of the Order of Australia (AC) for his ‘eminent service to science, and to higher education, particularly in the fields of polymer chemistry and materials science, through seminal contributions as a research innovator, as a mentor, and to the community.